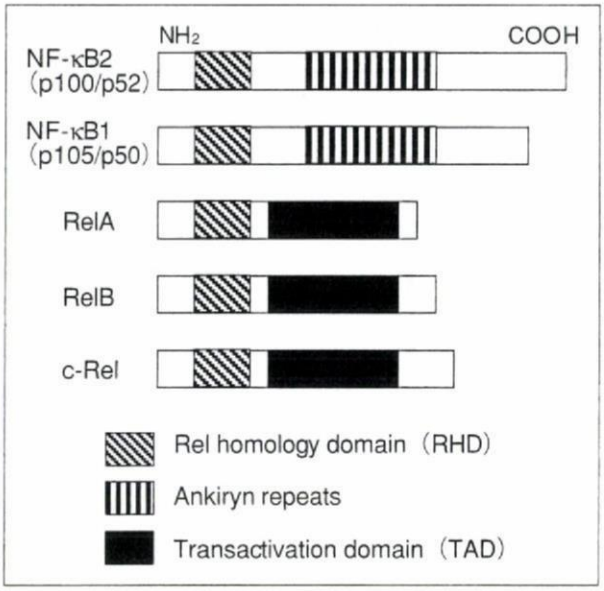


図1　NF-κBサブユニットの構造

(PI3K)といったアダプター分子を介して，protein kinase C θ(PKCθ)，caspase-recruitment domain-containing membrane-associated guanylate kinase protein 1(CARMA1)のリン酸化へと進んでいく．PKCθより上流のシグナルはAP-1, NFATといったNF-κBとは別のルートによるT細胞の活性化経路と共通しているが，3-phosphoinositide-dependent protein kinase 1(PDK1)から引き続いて誘導されるPKCθとCARMA1のリン酸化はNF-κBの活性化に重要な起点となっている．PKCθのリン酸化に続いてCARMA1, B-cell lymphoma 10 (Bcl-10)，mucosa-associated-lymphoid-tissue lymphoma-translocation gene 1(MALT-1)複合体を介してIκB kinase(IKK)の活性化につながっていく[5)6)]．また，PKCθが直接IKKに結合してIKKの活性を調節していることも明らかにされている[7)]．一方，副刺激分子であるCD28からのシグナルに関しては，TCRの刺激がない状態でCD28刺激を入れてもNF-κBの活性化は不十分であり，T細胞の活性化および増殖といった正常な機能獲得には至らない．CD28分子からのシグナルはTCRの下流のPI3KやAKTなどのアダプター分子を経由して上記のPKC/CARMA1/Bcl-10/MALT-1を介してIKKの活性化につながり，TCRからのNF-κBシグナルを量的に調節しているものと考えられる．IL-2レセプターなどのサイトカインレセプターからのシグナルに関してもTCRの下流のシグナル分子と合流していることが知られている[8)9)]．

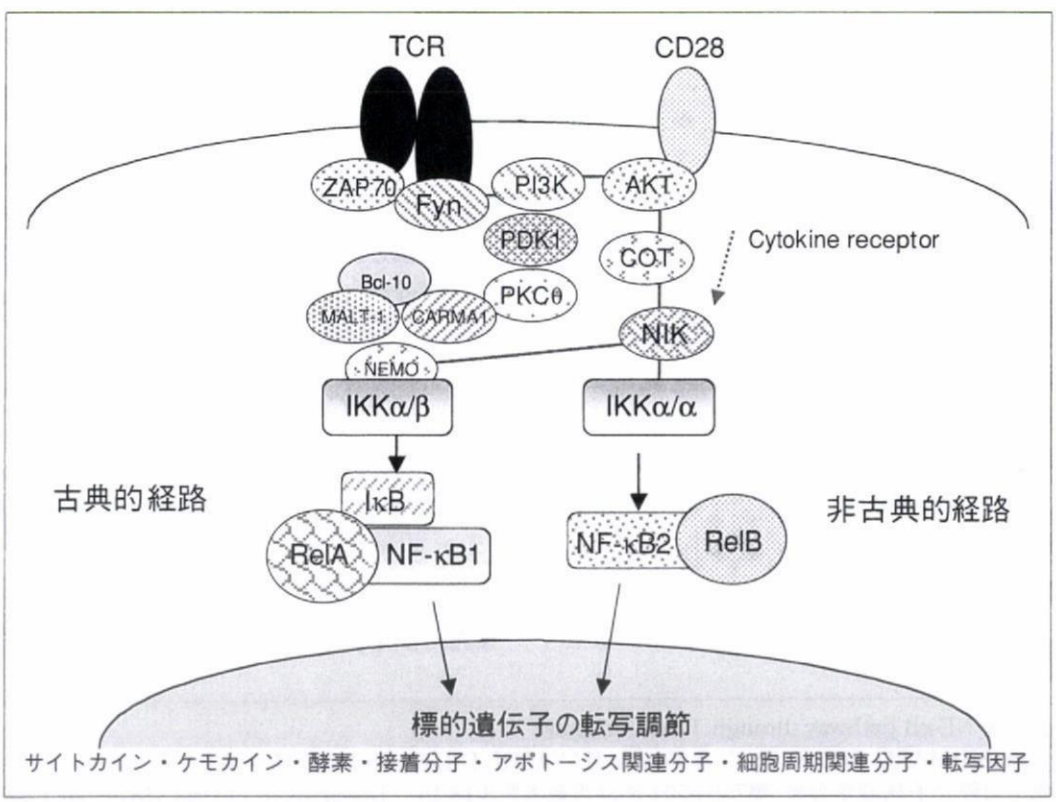


図2　T細胞レセプターと古典的NF-κB経路および非古典的(新規)NF-κB経路
T細胞あるいはCD28の下流におけるNF-κBの転写活性に至る過程の概略図を示す．

## IκBによる制御システム

NF-κBの活性化の引き金となるのが，NF-κB分子と結合しているIκBのリン酸化から始まるユビキチン化，断片化である．通常はNF-κB分子は細胞質でIκBと結合することによって核内に移行しないように制御されている[5]．CARMA1/Bcl-10/MALT-1複合体の活性化からIKKのキナーゼ活性が高まりIκBのリン酸化が誘導されると，IκB分子はユビキチン化を受けた後プロテアソームにより分断化されることによりNF-κBの核内移行を阻害できなくなる．つまり，IκBによる制御が解除されるときにNF-κBの活性化は開始される．正常マウスのCD4陽性T細胞を抗TCR抗体および抗CD28抗体により刺激すると，IκBのリン酸化および断片化，さらに，NF-κB分子の核内移行が観察される(図3)．IκB分子をリン酸化するのがIKK複合体であり，2つのキナーゼと調節蛋白であるNF-κB essential molecule(NEMO)から構成されるIKKはCARMA1/Bcl-10/MALT-1を介してNEMOのユビキチン化，IKKαまたはIKKβのリン酸化を通したキナーゼ活性の上昇によりIκBのリン酸化に結びついていく[10]．シグナルを制御する分子を各ステップで解除していくことにより，NF-κBの活性化が開始される．逆に言えば，NF-κBはいくつもの制御システムにより精巧に調節されていると言ってよい．ひとたび，NF-κB分子が核内に移行するとT細胞の機能にきわめて重要な遺伝子の転写調節が進行するのである．

## NF-κBの核内移行

NF-κB分子が核内移行すると標的遺伝子のプロモーター領域に存在するκB結合部位にNF-κB分子が直接結合することにより，その遺伝子の転写活性が開始される．5つのNF-κBサブユニットの中で実際に標的遺伝子の転写を司るのはC末に転写活性領域を有するRelA(p65)，RelB, c-Relである(図1)．一方，NF-κB1(p105/p50)とNF-κB2(p100/p52)には転写活性領域は存在しないが，核内移行に重要なシグナルモチーフを有していることから，NF-κB1およびNF-κB2は他の3つのサブユニットとのヘテロダイマーの形成により核内移行を最終的に調節していると考えられる[3]．NF-κBはT細胞の活性化や増殖に重要なIL-2およびその受容体の一つであるCD25などのようなサイトカインやサイトカイン受容体，ケ

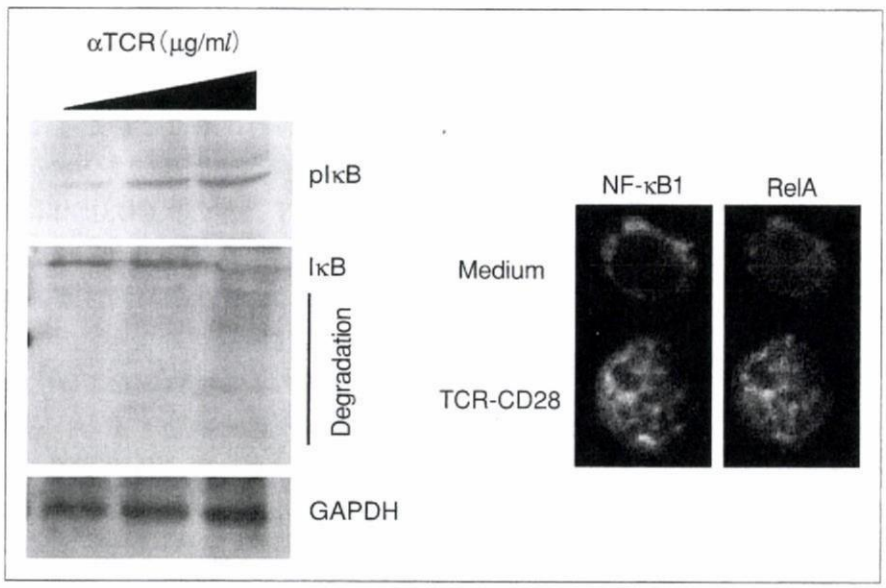


図3 NF-κBの活性化

左：正常マウス脾臓からのCD4陽性細胞に抗TCR抗体(0～1μg/ml)および抗CD28抗体(20μg/ml)で刺激し，抗リン酸化IκB抗体によりウエスタンブロットを行った．さらに，IκBの断片化を確認した．ローディングコントロールとしてglyceraldehyde phosphate dehydrogenase(GAPDH)を用いた．

右：刺激後のCD4陽性T細胞のNF-κB1およびRelAの核内移行をコンフォーカル顕微鏡解析により確認した．

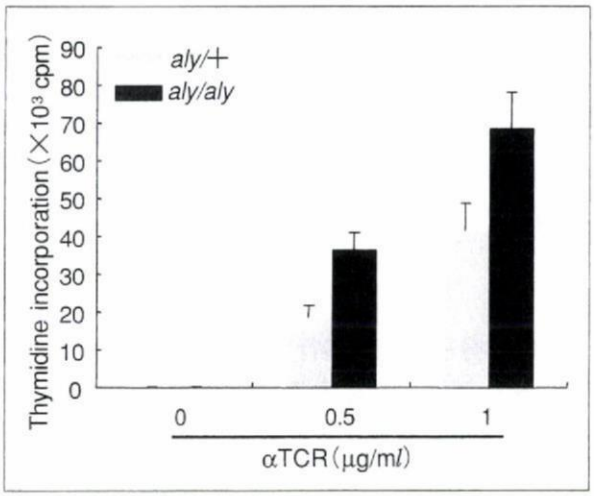


図4　NF-κB2不全マウスのナイーブT細胞の反応性
*aly/aly*マウスと対照マウスの脾臓CD4陽性細胞に抗TCR抗体(0～1 μg/ml)および抗CD28抗体(20μg/ml)で48時間刺激し，培養の最終12時間における[³H]標識チミジンの取り込みをシンチレーションカウンターにより計測した．

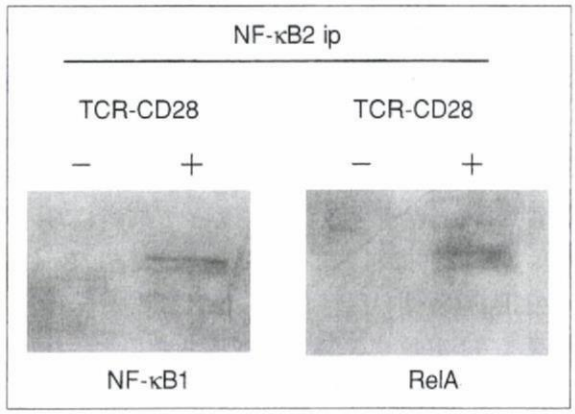


図5　NF-κB2分子とNF-κB1およびRelAとの結合
正常マウス脾臓からのCD4陽性細胞に抗TCR抗体(1 μg/ml)および抗CD28抗体(20μg/ml)で刺激し，細胞質分画蛋白質を抽出後，NF-κB2抗体で免疫沈降(ip)を行い，ウエスタンブロット法によりNF-κB1およびRelAを検出した．

モカイン，接着分子，アポトーシス関連因子，細胞周期関連因子などT細胞の分化，維持および機能獲得に重要な遺伝子群を標的としている[11]．さらに，NF-κB遺伝子自体をNF-κBが転写調節していることが知られており，転写因子自体の発現調節を自身で制御しているという点はNF-κBそのものの動態を知る上で重要である[12]．また，各サブユニットがどの標的遺伝子の転写調節に関連しているのかの区別は明確にできていない．各サブユニットの組み合わせや，シグナルカスケードの各中継ポイントにおけるシグナルの質的および量的な違いなど複雑な因子の影響によりNF-κBの活性システムが調節されていることが想定される．

## T細胞における非古典的経路

では，T細胞の活性化に非古典的NF-κB経路は関与してないのであろうか．NF-κB2およびRelBの遺伝子欠損マウスでもT細胞に機能不全や自己免疫病変の発症が報告されている[13][14]．

正常マウスのCD4陽性T細胞への抗TCR抗体および抗CD28抗体による活性化におけるNF-κBの動態を観察すると，活性の初期段階ではNF-κB1/RelAのヘテロダイマーの核内移行が中心であり，非古典的経路であるNF-κB2/RelBの核内移行はほとんど認められず，増殖期を含む後期段階ではNF-κB2/RelBの核内移行が確認されるが[15]，その役割は不明であった．非古典的NF-κB経路ではTCRおよびCD28からのシグナル伝達に関しては古典的経路ほど明らかにされていない．PKCθ，PI3KおよびAKTからNF-κB-inducing kinase(NIK)を活性化し，NIKはIKKαをリン酸化することによりNF-κB2(p100)のIκB様配列をリン酸化，ユビキチン化する．古典的NF-κB経路と同様にプロテアソームにより断片化され，p52にプロセッシングされることによりp52/RelBヘテロダイマーが核内に移行することが知られている[3]．NIK遺伝子の点変異マウスである*aly/aly*マウスは末梢CD4陽性T細胞の抗CD3抗体による増殖反応が対照マウスに比較して低下していることが報告されているが[16]，CD4陽性T細胞の中で，メモリー型のT細胞を除去し，ナイーブ型のCD4陽性T細胞のみを抗TCRおよび抗CD28抗体で刺激して増殖反応を観察すると，対照マウスに比較して有意に高い反応性が認められた(図4)．一方で，*aly/aly*マウスのメモリー型のみの増殖反応はきわめて低くなっていることが判明した[15]．NIK欠損マウスにおいてもナイーブ型CD4陽性T細胞の増殖活性は有意に上昇していることを確認した．さらに，NF-κB2欠損マウスにおいてもT細胞の過剰増殖が報告されていることから，ナイーブCD4陽性T細胞の活性化における非古典的NF-κB経路(NF-κB2/RelB)の負の制御機構が存

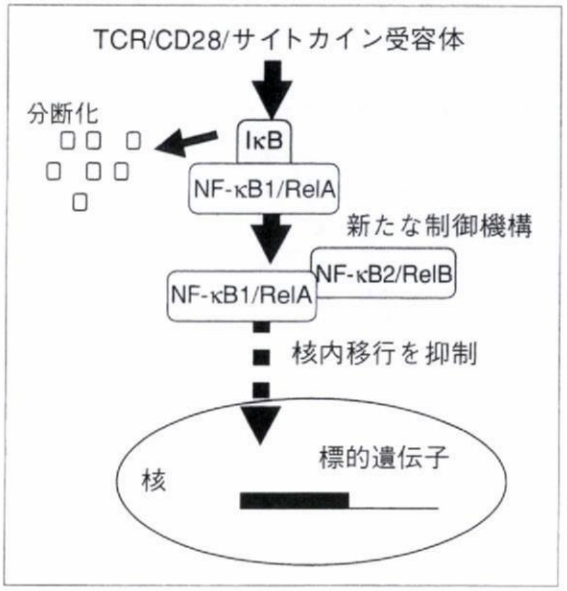


図6 NF-κB2による古典的NF-κB経路の新たな制御機構

在することが明らかになった．また，T細胞のナイーブからメモリー型に至る段階でNF-κBのサブユニットの役割が分担されている可能性が示された．

## NF-κBサブユニット間のクロストーク

NF-κBのサブユニット間での結合に関しては，RelA, RelBおよびc-Relでのホモダイマー以外は5つのサブユニット間でヘテロダイマー，ホモダイマーを形成しうることが知られているが，それらのT細胞における生理的および機能的役割は明らかにされていなかった．上述のNF-κB2の制御機構の細胞内での機序を知るために，正常マウスからナイーブ型($CD44^{low}$)のCD4陽性T細胞を用いて抗TCRおよび抗CD28抗体で刺激した後に，細胞質分画の蛋白質を抽出し，NF-κB2抗体で免疫沈降して各NF-κBサブユニットに対する抗体でウエスタンブロット法により各サブユニットとNF-κB2の直接の結合を確認したところ，NF-κB1およびRelA蛋白が検出された(図5)．一方，*aly/aly*マウスではナイーブ型CD4陽性細胞に刺激を加えると，NF-κB2の合成が阻害されることも判明し，NF-κB2とNF-κB1およびRelAとの結合は観察されなかった[15]．この所見は*aly/aly*マウスのナイーブ型CD4陽性T細胞の過剰な反応性がNF-κB2分子を介した制御機構の異常により生じていることを示唆している．従来のIκBによるNF-κBの活性化制御機構に加え，NF-κB2分子がNF-κB1/RelA複合体と細胞質で直接結合することにより，その複合体の核内移行を阻害することでNF-κBの活性化シグナルを調節する新たな免疫制御機構が明らかにされた(図6)．一方で，メモリー型($CD44^{high}$)CD4陽性T細胞に関してはこの制御システムは働いていないことから，T細胞の活性化段階でNF-κBの各サブユニットの役割が異なっている可能性が示された．非古典的NF-κB経路と古典的NF-κB経路のクロストークはT細胞のみではなく，たとえば，破骨細胞の活性化過程においても報告されていることから，別の細胞種においても，このシステムがなんらかの機能調節に関与している可能性がある[12)17)]．

## NF-κBと免疫疾患

これまでにNF-κB各サブユニットの遺伝子欠損マウスの解析からT細胞におけるNF-κBの生体内での役割が明らかにされている．たとえば，NF-κB1欠損マウスのT細胞では増殖の抑制および$Th_2$タイプのサイトカインの産生減少が観察され，ヒト多発性硬化症の疾患モデル(EAE)での病態感受性の上昇および*Leishmania major*への易感染性がみられ，また，RelA欠損マウスは胎生致死であるが，胎児肝細胞キメラを用いた実験でT細胞の機能低下が報告されている[18)~22)]．一方，RelB欠損マウスは2～3か月齢で重度の自己免疫性貧血および全身の炎症で死亡し，T細胞の機能低下も観察されている[13)]．さらに，NF-κB2欠損マウスではT細胞の過反応がみられ，c-Rel欠損マウスではT細胞の反応性の低下やEAEに対する疾患感受性の低下が知られている[23)24)]．加えて，NF-κB2分子を調節する因子であるNIKの欠損マウスおよびNIK遺伝子の変異マウスにおいてT細胞の増殖は抑制され，多臓器に自己免疫病変が発症することが報告されている[25)]．しかし，T細胞の各活性化段階でのNF-κBの詳細な役割や各サブユニット同士の相互作用と自己免疫との関係は不明な点が多かった．

*aly/aly*マウスやNIK欠損マウスにおける自己免疫病変の発症には胸腺由来の$CD25^+CD4^+$調節性T細胞の数的な減少および質的な障害が自己免

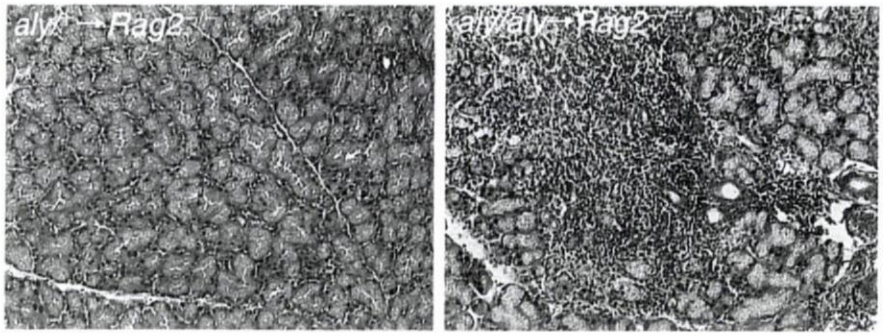


図7　NF-κB2機能不全と自己免疫
*aly/aly*マウスと対照マウスのナイーブ型CD4陽性T細胞を*Rag2*遺伝子欠損マウスに移入後6週における涙腺の病理組織像を示す．*aly/aly*→*Rag2*$^{-/-}$群では腺組織の破壊を伴ったリンパ球浸潤が認められる．

疫の発症に重要であることが報告されている[16)26)]．しかし，*aly/aly*マウスのナイーブ型CD25$^{-}$CD4$^{+}$T細胞を*Rag2*遺伝子欠損マウスに移入すると，本来の*aly/aly*マウスに発症する自己免疫病変よりもはるかに激しい自己免疫性病変が肺や涙腺に認められたことから，調節性T細胞の制御異常に加えて，NF-κB2によるT細胞の制御機構に障害をきたすと自己免疫疾患の発症に結びつくことが示された(図7)．

## ま と め

Nuclear factor(NF)-κBによる標的遺伝子の転写活性システムはT細胞にとって必須であるといえる．しかし，5つのサブユニットでどれが重要であるのかはいまだ解明されていない．NF-κBのサブユニット遺伝子のそれぞれの欠損マウスの中にはT細胞の分化や末梢トレランスは正常に維持され，T細胞になんらかの刺激が加えられたときにのみ特定の機能に異常が生じている場合がある．また，なんら機能的異常が見出せない場合も報告されている．サブユニットのどれかが欠損しても別のサブユニットが代替的に機能していることも考えられる．実際の免疫反応においてもT細胞にとってNF-κBシグナルに障害が生じれば，別のサブユニットが動員され，過剰なシグナルが伝われば各サブユニットを介して制御的に働くNF-κBネットワークシステムが免疫トレランスの維持に働いているのではなかろうか．今後，NF-κBシグナルと免疫疾患との関係を明らかにすることは臨床的にもきわめて有用であるといえる．

## 文　献

1) Karin M, Ben-Neriah Y. Phosphorylation meets ubiquitination : the control of NF-κB activity. Annu Rev Immunol 2000 ; 18 : 621.
2) Karin M. How NF-kappaB is activated : the role of the IkappaB kinase (IKK) complex. Oncogene 1999 ; 18 : 6867.
3) Bonizzi G, Karin M. The two NF-kappaB activation pathways and their role in innate and adaptive immunity. Trends Immunol 2004 ; 25 : 280.
4) Kahn-Perles B, Lipcey C, Lecine P, et al. Temporal and subunit-specific modulations of the Rel/NF-kappaB transcription factors through CD28 costimulation. J Biol Chem 1997 ; 272 : 21774.
5) Sun Z, Arendt CW, Ellmeier W, et al. PKC-theta is required for TCR-induced NF-kappaB activation in mature but not immature T lymphocytes. Nature 2000 ; 404 : 402.
6) Lee K, D'Acquisto F, Hyden M, et al. PDK1 nucleates T cell receptor-induced signaling complex for NF-κB activation. Science 2005 ; 308 : 114.
7) Trushin SA, Pennington KN, Algeciras-Schimnich A, et al. Protein kinase C and calcineurin synergize to activate IκB kinase and NF-κB in T lymphocytes. J Biol Chem 1999 ; 274 : 22923.
8) Pimentel-Muinos FX, Mazana J, Fresno M. Regulation of interleukin-2 alpha chain expression and nuclear factor kappa B activation by protein kinase C in T lymphocytes. Autocrine role of tumor necrosis factor alpha. J Biol Chem 1994 ; 269 : 24424.

9) Prasad AS, Bao B, Beck FW, et al. Zinc enhances the expression of interleukin-2 and interleukin-2 receptors in HUT-78 cells by way of NF-kappaB activation. J Lab Clin Med 2002 ; 140 : 272.
10) Rawlings DJ, Sommer K, Moreno-Garcia ME. The CARMA1 signalosome links the signaling machinery of adaptive and annate immunity in lymphocytes. Nat Rev Immunol 2006 ; 6 : 799.
11) Hayden MS, West AP, Ghosh S. NF-κB and immune response. Oncogene 2006 ; 25 : 6758.
12) Novack DV, Yin L, Hagen-Stapleton A, et al. The IkappaB function of NF-kappaB2 p100 controls stimulated osteoclastogenesis. J Exp Med 2003 ; 198 : 771.
13) Weih F, Carrasco D, Durham SK, et al. Multiorgan inflammation and hematopoietic abnormalities in mice with a targeted disruption of RelB, a member of the NF-kappa B/Rel family. Cell 1995 ; 80 : 331.
14) Kajiura F, Sun S, Nomura T, et al. NF-kappa B-inducing kinase establishes self-tolerance in a thymic stroma-dependent manner. J Immunol 2004 ; 172 : 2067.
15) Ishimaru N, Kishimoto H, Hayashi Y, et al. Regulation of naïve T cell function by the NF-κB2 pathway. Nat Immunol 2006 ; 7 : 763.
16) Matsumoto M, Yamada T, Yoshinaga SK, et al. Essential role of NF-kappa B-inducing kinase in T cell activation through the TCR/CD3 pathway. J Immunol 2002 ; 169 : 1151.
17) Speirs K, Lieberman L, Caamano J, et al. Cutting edge : NF-kappa B2 is a negative regulator of dendritic cell function. J Immunol 2004 ; 172 : 752.
18) Artis D, Speirs K, Joyce K, et al. NF-kappa B1 is required for optimal $CD4^+$ Th1 cell development and resistance to *Leishmania major*. J Immunol 2003 ; 170 : 1995.
19) Erdman S, Fox JG, Dangler CA, et al. Typhlocolitis in NF-kappa B-deficient mice. J Immunol 2001 ; 166 : 1443.
20) Hilliard B, Samoilova EB, Liu TS, et al. Experimental autoimmune encephalomyelitis in NF-kappa B-deficient mice : roles of NF-kappa B in the activation and differentiation of autoreactive T cells. J Immunol 1999 ; 163 : 2937.
21) Beg AA, Sha WC, Bronson RT, et al. Embryonic lethality and liver degeneration in mice lacking the RelA component of NF-kappa B. Nature 1995 ; 376 : 167.
22) Doi T, Takahashi T, Taguchi O, et al. NF-κB RelA-deficient lymphocytes : Normal development of T cells and B cells, impaired production of IgA and IgG1 and reduced proliferative responses. J Exp Med 1997 ; 185 : 953.
23) Hilliard BA, Mason N, Xu L, et al. Critical roles of c-Rel in autoimmune inflammation and helper T cell differentiation. J Clin Invest 2002 ; 110 : 843.
24) Franzoso G, Carlson L, Poljak L, et al. Mice deficient in nuclear factor (NF)-kappa B/p52 present with defects in humoral responses, germinal center reactions, and splenic microarchitecture. J Exp Med 1998 ; 187 : 147.
25) Tsubata R, Tsubata T, Hiai H, et al. Autoimmune disease of exocrine organs in immunodeficient alymphoplasia mice : a spontaneous model for Sjogren's syndrome. Eur J Immunol 1996 ; 26 : 2742.
26) Lu L, Gondek DC, Scott ZA, et al. NF-κB-inducing kinase deficiency results in the development of a subset of regulatory T cells, which shows a hyperproliferative activity upon glucocorticoid-induced TNF receptor family-related gene stimulation. J Immunol 2005 ; 175 : 1651.

* * *

# Visualizing the dynamics of p21$^{Waf1/Cip1}$ cyclin-dependent kinase inhibitor expression in living animals

Naoko Ohtani*†, Yuko Imamura*, Kimi Yamakoshi*, Fumiko Hirota‡, Rika Nakayama§, Yoshiaki Kubo¶, Naozumi Ishimaru¶, Akiko Takahashi*, Atsushi Hirao‖**, Takatsune Shimizu††, David J. Mann‡‡, Hideyuki Saya††, Yoshio Hayashi¶, Seiji Arase¶, Mitsuru Matsumoto‡, Kazuki Nakao§, and Eiji Hara*†

*Institute for Genome Research, ‡Institute for Enzyme Research, and ¶Institute of Health Biosciences, University of Tokushima, Tokushima 770-8503, Japan; §Center for Developmental Biology, RIKEN, Kobe 650-0047, Japan; ‖Cancer Research Institute, Kanazawa University, Kanazawa 920-0934, Japan; **CREST, Japan Science and Technology Agency, Tokyo 102-0075, Japan; ††Institute for Advanced Medical Research, Keio University School of Medicine, Tokyo 160-8582, Japan; and ‡‡Division of Cell and Molecular Biology, Imperial College London, London SW7 2AZ, United Kingdom

Communicated by Thaddeus P. Dryja, Harvard Medical School, Boston, MA, July 25, 2007 (received for review May 11, 2007)

**Although the role of *p21$^{Waf1/Cip1}$* gene expression is well documented in various cell culture studies, its *in vivo* roles are poorly understood. To gain further insight into the role of *p21$^{Waf1/Cip1}$* gene expression *in vivo*, we attempted to visualize the dynamics of *p21$^{Waf1/Cip1}$* gene expression in living animals. In this study, we established a transgenic mice line (p21-*p*-luc) expressing the firefly luciferase under the control of the *p21$^{Waf1/Cip1}$* gene promoter. In conjunction with a noninvasive bioluminescent imaging technique, p21-*p*-luc mice enabled us to monitor the endogenous *p21$^{Waf1/Cip1}$* gene expression *in vivo*. By monitoring and quantifying the *p21$^{Waf1/Cip1}$* gene expression repeatedly in the same mouse throughout its entire lifespan, we were able to unveil the dynamics of *p21$^{Waf1/Cip1}$* gene expression in the aging process. We also applied this system to chemically induced skin carcinogenesis and found that the levels of *p21$^{Waf1/Cip1}$* gene expression rise dramatically in benign skin papillomas, suggesting that *p21$^{Waf1/Cip1}$* plays a preventative role(s) in skin tumor formation. Surprisingly, moreover, we found that the level of *p21$^{Waf1/Cip1}$* expression strikingly increased in the hair bulb and oscillated with a 3-week period correlating with hair follicle cycle progression. Notably, this was accompanied by the expression of p63 but not p53. This approach, together with the analysis of *p21$^{Waf1/Cip1}$* knockout mice, has uncovered a novel role for the *p21$^{Waf1/Cip1}$* gene in hair development. These data illustrate the unique utility of bioluminescence imaging in advancing our understanding of the timing and, hence, likely roles of specific gene expression in higher eukaryotes.**

aging | cell cycle | hair cycle | imaging

The founding member of the mammalian cyclin-dependent kinase (CDK) inhibitor family, p21$^{Waf1/Cip1}$, is one of the best characterized transcriptional targets of the p53 tumor suppressor protein (1–4). As a general inhibitor of CDKs, p21$^{Waf1/Cip1}$ prevents phosphorylation of the retinoblastoma tumor suppressor protein (pRb) thereby enhancing its growth suppressive function (2, 3, 5). Thus, p21$^{Waf1/Cip1}$ links the p53 pathway to the pRb pathway, providing a tight security network toward tumor suppression. Indeed, the tumor-suppressive role of p21$^{Waf1/Cip1}$ is well documented in various cell culture studies; up-regulation of the *p21$^{Waf1/Cip1}$* gene expression participates in processes such as DNA damage-induced cell cycle arrest, cellular senescence, and terminal differentiation, each of which may prevent tumor formation (5, 6). However, *in vivo*, the role of p21$^{Waf1/Cip1}$, especially in the context of tumor suppression, remains unclear. For example, mutations in the *p21$^{Waf1/Cip1}$* gene are rarely observed in human cancers (7), and, although the majority of mice lacking the *p53* gene develop spontaneous tumors by 6 months of age (8, 9), mice lacking the *p21$^{Waf1/Cip1}$* gene do not exhibit any predisposition to spontaneous tumor formation (10, 11). These observations raise a question of whether the results seen in cell culture truly reflect the physiological roles of p21$^{Waf1/Cip1}$ *in vivo*. However, because knockout experiments performed to date have used mice with germ-line deficiencies at the *p21$^{Waf1/Cip1}$* gene locus, there is the possibility of developmental compensation, as seen with other cell cycle regulators (12, 13). Moreover, expression of the *p21$^{Waf1/Cip1}$* gene overlaps with that of other CDK inhibitor family members in many different tissues (5). It is, therefore, possible that the effects of *p21$^{Waf1/Cip1}$* deficiency is somewhat compromised by developmental or somatic compensation by functionally related CDK inhibitors in *p21$^{Waf1/Cip1}$* knockout mice. Alternative approaches are therefore needed to supplement the *in vitro* studies and assist in understanding the physiological roles of *p21$^{Waf1/Cip1}$* gene expression *in vivo*.

Bioluminescence imaging (BLI) is an emerging approach that is based on detection of light emission from cells or tissues (14, 15). Optical imaging by bioluminescence allows a noninvasive and real-time analysis of various biological responses, such as gene expression, proteolytic processing, or protein–protein interactions, in living animals (16–20). In this study, we generated a transgenic mice line (p21-*p*-luc) expressing the firefly luciferase under the control of the *p21$^{Waf1/Cip1}$* gene promoter. Using this mouse model, we explored the dynamics of *p21$^{Waf1/Cip1}$* gene expression in many different biological processes *in vivo*. This approach, in conjunction with the analysis of *p21$^{Waf1/Cip1}$* knockout mice, uncovered a previously uncharacterized function of *p21$^{Waf1/Cip1}$* gene expression in hair development. The ability to image *p21$^{Waf1/Cip1}$* gene expression noninvasively therefore provides a valuable tool for studies on the role of *p21$^{Waf1/Cip1}$* gene expression *in vivo*.

## Results

To study how *p21$^{Waf1/Cip1}$* gene expression is regulated *in vivo*, we attempted to visualize the transcriptional activity of the *p21$^{Waf1/Cip1}$* gene in living animals. To this end, a transgenic mice line (p21-*p*-luc mice) expressing the firefly luciferase

Author contributions: N.O. and Y.I. contributed equally to this work; N.O. and E.H. designed research; N.O., Y.I., K.Y., F.H., R.N., Y.K., N.I., A.T., A.H., and T.S. performed research; N.O., D.J.M., H.S., Y.H., S.A., M.M., K.N., and E.H. analyzed data; and N.O. and E.H. wrote the paper.

The authors declare no conflict of interest.

Freely available online through the PNAS open access option.

Abbreviations: CDK, cyclin-dependent kinase; pRb, retinoblastoma tumor suppressor protein; BLI, bioluminescence imaging.

†To whom correspondence may be addressed. E-mail: ohtani@genome.tokushima-u.ac.jp or hara@genome.tokushima-u.ac.jp.

This article contains supporting information online at www.pnas.org/cgi/content/full/0706949104/DC1.

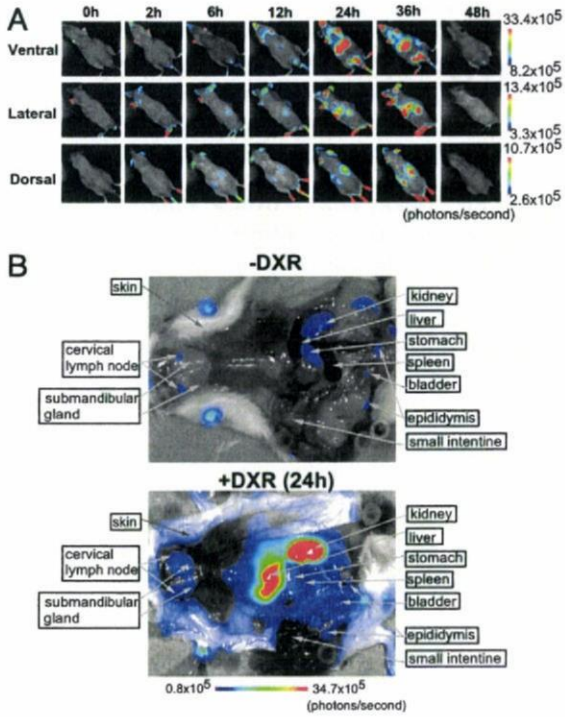


**Fig. 1.** Characterization of the p21-*p*-luc mice. (*A*) The p21-*p*-luc mice (8-week-old) were injected i.p. with doxorubicin (DXR) (20 mg/kg) and were subjected to noninvasive BLI at various times after doxorubicin (DXR) injection. Representative images of five different experiments are shown. (*B*) The same line of p21-*p*-luc mice were treated with doxorubicin (+DXR) (20 mg/kg) or saline (−DXR) for 24 h, injected with luciferin, and incised through the mouth and anus under anesthesia. Representative BLI data of five different experiments are shown. The color bar indicates photons with minimum and maximum threshold values.

driven by the $p21^{Waf1/Cip1}$ gene promoter, which contains two p53-binding sites, was established and subjected to noninvasive *in vivo* BLI. Although basal levels of bioluminescent signals were very low throughout the body, except for the paws, a striking increase in signal was observed (particularly over the abdomen) within 24 h of treatment with doxorubicin, a DNA damaging agent that activates p53 (Fig. 1*A*). These signals were sustained until 36 h and then declined to baseline values within the next 12 h (Fig. 1*A*, 48 h). To define the organs expressing high levels of luciferase activity, the same lines of transgenic mice were treated with or without doxorubicin for 24 h, injected with luciferin, and incised through mouth and anus under anesthesia (Fig. 1*B*). As expected from noninvasive BLI data (Fig. 1*A*, 24 h), a significant induction of bioluminescent signal was observed in liver and kidney in doxorubicin-treated mice [Fig. 1*B* and supporting information (SI) Fig. 4*A*]. A substantial but less pronounced induction was observed in the submandibular gland, spleen, bladder, and stomach (Fig. 1*B* and SI Fig. 4*A*). Similar but different dynamics of $p21^{Waf1/Cip1}$ gene expression was observed by x-ray irradiation (SI Fig. 5). Importantly, the levels of bioluminescent signal were well correlated with those of endogenous $p21^{Waf1/Cip1}$ mRNA (SI Figs. 4 and 5), indicating that, in the p21-*p*-luc mice, luciferase expression accurately reports the transcriptional dynamics of $p21^{Waf1/Cip1}$ gene expression *in vivo*. Furthermore, in concordance with the levels of endogenous $p21^{Waf1/Cip1}$ expression, luciferase activity was strikingly increased in the cortex and medulla of the kidney (SI Fig. 6). Taken together, these results suggest that the p21-*p*-luc mice provide an ideal tool for the analysis of $p21^{Waf1/Cip1}$ gene expression *in vivo*.

Although p53 serves the beneficial function of tumor suppression, p53 activation may, in some circumstance, act in a manner detrimental to the long-term homeostasis of living organism (21). Indeed, aberrant activation of p53 is known to accelerate the aging process in mice, and the induction of $p21^{Waf1/Cip1}$ gene expression has been shown to be involved this process (22, 23). We thus next attempted to explore the dynamics of $p21^{Waf1/Cip1}$ gene expression throughout entire life span in p21-*p*-luc mice (SI Fig. 7). Unexpectedly, only a slight (3- to 4-fold) induction of bioluminescent signal was observed in aged kidney but not in other aged organs or tissues (SI Fig. 7). Surprisingly, moreover, any signs of strong activation of p53 and DNA damage responses were not observed in aged kidney (SI Fig. 7), indicating that the induction of $p21^{Waf1/Cip1}$ gene expression in aged kidney is likely to be regulated by a p53-independent mechanism, although we cannot rule out the possibility that weak activation of p53 contributes to the up-regulation of $p21^{Waf1/Cip1}$ gene expression.

The up-regulation of $p21^{Waf1/Cip1}$ gene expression is implicated in cellular senescence, the state of stable cell cycle arrest provoked by diverse stresses including DNA damage and oncogenic *ras* expression in cultured primary cells (4, 24). To explore this notion *in vivo*, p21-*p*-luc mice were subjected to a conventional chemically induced skin tumor protocol with a single dose of DMBA for initiation and biweekly treatment with 12-*o*-tetradecanoylphorbol 13-acetate (TPA) for promotion. Because this protocol causes an oncogenic mutation in the H-*ras* gene, it appeared to be ideal for studying physiological responses against oncogenic *ras* expression in living animals (25, 26). In agreement with previous reports (25, 26), benign skin papillomas began to appear after 7–8 weeks of promotion (Fig. 2*A*). Notably, papilloma formation was accompanied by the induction of a bioluminescence signal (Fig. 2*A*), endogenous $p21^{Waf1/Cip1}$ expression, and activation of p53 (Fig. 2*B*). These observations, together with previous studies that indicate that disruption of the $p21^{Waf1/Cip1}$ gene results in an increase of papilloma formation or carcinoma formation (27–29), strongly suggest that $p21^{Waf1/Cip1}$ plays a preventative role against oncogenic *ras*-signaling *in vivo*.

Because noninvasive BLI permits continuous readout of gene expression in living animals (14, 15), we next examined the kinetics of $p21^{Waf1/Cip1}$ gene expression toward papilloma formation. To our surprise, a remarkable bioluminescent signal was observed well before papilloma appearance and oscillated with a 3-week period (Figs. 2 *C* and *D*). Unexpectedly, moreover, a remarkable expression of endogenous $p21^{Waf1/Cip1}$ was observed in the hair bulb, but not in the skin itself (Fig. 2*E*), suggesting that $p21^{Waf1/Cip1}$ may play a role in hair development. To produce new hairs, existing hair follicles undergo cycles of growth (anagen), regression (catagen), and rest (telogen) (30). Because TPA treatment has been shown to promote entry of hair follicles into their anagen phase (31), we next asked whether the oscillating bioluminescence signal in DMBA/TPA-treated skin reflects hair follicle cycle progression. Although TPA treatment, in itself, did not cause skin papilloma formation, a similar oscillation of bioluminescence signals and $p21^{Waf1/Cip1}$ mRNA expression was induced by TPA treatment alone (SI Fig. 8). Notably, this was accompanied by remarkable hair growth (SI Fig. 8*A*), suggesting a role for $p21^{Waf1/Cip1}$ in the hair follicle cycle progression in mouse skin.

To substantiate this idea in a more physiological setting, we next tested whether $p21^{Waf1/Cip1}$ expression oscillates throughout the natural hair follicle cycle, exploiting the fact that hair follicle cycles are synchronized for the first two postnatal periods of hair follicle growth in mice (32). Although the dynamics of hair cycle progression were visually undetectable during the second postnatal hair follicle cycle, BLI was sensitive enough to monitor oscillating $p21^{Waf1/Cip1}$ expression (Fig. 3*A*). The levels of biolu-

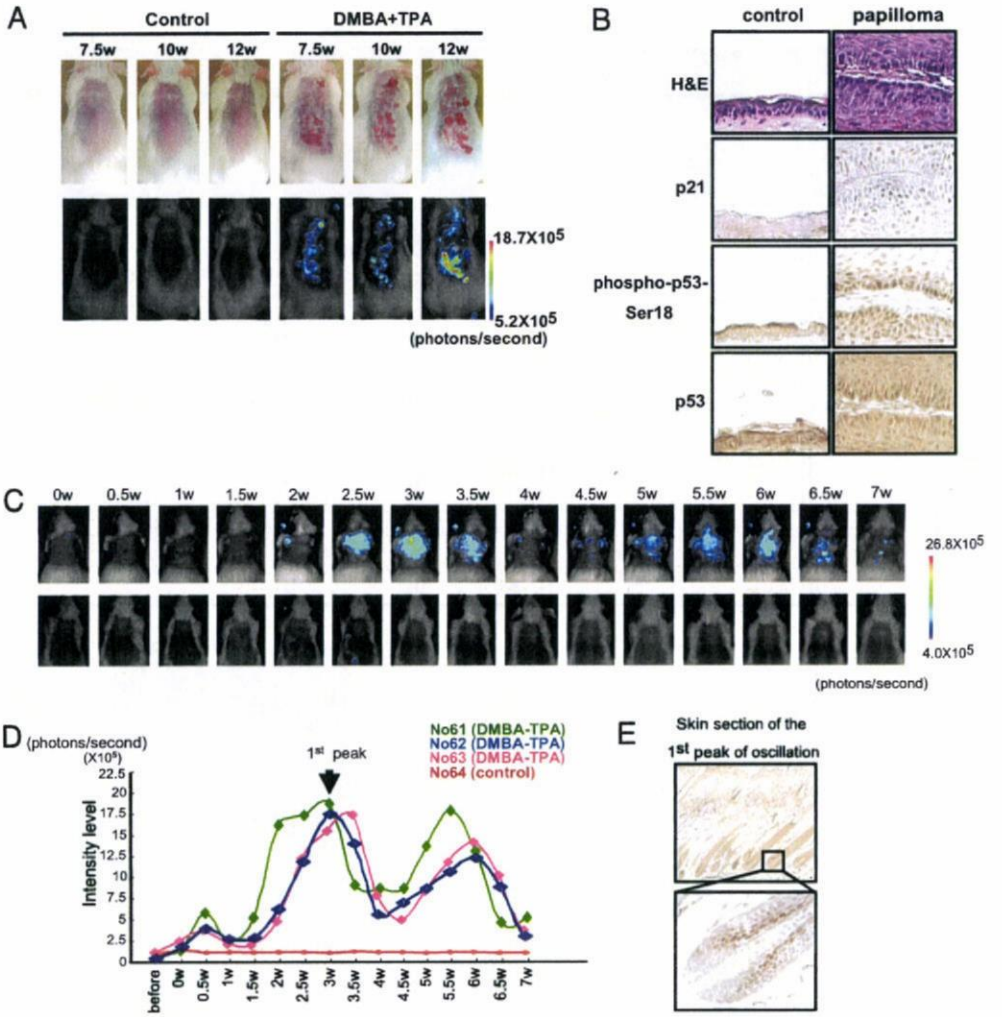


Fig. 2. Oscillation of bioluminescence signals in DMBA/TPA-treated mouse skin. (*A*) The p21-*p*-luc mice treated with DMBA/TPA or with acetone (control) were subjected to noninvasive BLI at indicated time points after TPA treatment. Representative images of 12 different experiments were shown (*Lower*). These papillomas and control skin were photographed in regular lighting (*Upper*). The color bar indicates photons with minimum and maximum threshold values. (*B*) H&E staining and the immunohistochemistry for endogenous $p21^{Waf1/Cip1}$ expression, phosphorylation of p53 at serine 18 residue, and p53 expression were performed by using biopsy samples of skin papilloma (*Right*) or control normal skin (*Left*). (*C*) Noninvasive BLI was performed throughout the time course after DMBA/TPA treatment (*Upper*) or acetone control (*Lower*). Mice were imaged at 0.5-week intervals after TPA treatment. Representative images of 12 different experiments were shown. The color bar indicates photons with minimum and maximum threshold values. (*D*) The intensity of bioluminescence signal throughout the time course was graphed. (*E*) Immunohistochemistry was conducted to examine the endogenous $p21^{Waf1/Cip1}$ expression in the dorsal skin at 3 weeks after TPA treatment (corresponding to the first peak of bioluminescence oscillation). A magnified image of hair bulb is shown (*Lower*).

minescence signals reached their peak at postnatal day 28 (P28); endogenous $p21^{Waf1/Cip1}$ expression was also strongly observed in the precortex area above the hair matrix (differentiating cell area) at this time (Fig. 3*A*). These data suggest that $p21^{Waf1/Cip1}$ may regulate the size of hair bulb and thereby control the hair phenotype.

To explore this possibility, microscopic examination of the various hair types was conducted by using mice with different $p21^{Waf1/Cip1}$ genotypes (10). The morphology of the four main hair types (guard, awl, auchene, and zigzag) was not significantly different among three different genotypes ($p21^{+/+}$, $p21^{+/-}$, $p21^{-/-}$) (data not shown). However, the proportion of zigzag hairs, which are produced by the smallest hair bulb, was significantly reduced in $p21^{+/-}$ mice, whereas awl hairs and auchene hairs, which are produced by the intermediate-sized hair bulb, were increased (Fig. 3*B*). Curiously, these effects were less pronounced in $p21^{-/-}$ mice (Fig. 3*B*). Importantly, however, unusually high level of $p27^{Kip1}$ expression, another member of the $p21^{Waf1/Cip1}$ family CDK inhibitors, was observed in the hair bulb of $p21^{-/-}$ mice (Fig. 3*C*). Thus, it is likely that the effects of $p21^{Waf1/Cip1}$ deficiency are concealed, at least in part, by up-regulation of $p27^{Kip1}$ expression in the hair bulb of $p21^{-/-}$ mice. In line with this observation, the proportion of zigzag hairs has been shown to reduce in $p27^{Kip1}$ knockout mice (33), suggesting that $p21^{Waf1/Cip1}$ and $p27^{Kip1}$ possess overlapping role(s) in hair development.

It is worthwhile to note that a similar level of $p21^{Waf1/Cip1}$ expression was observed in anagen hair bulbs, regardless of p53 gene status (SI Fig. 9*A*). Moreover, the proportion of four main hair types was not substantially different among mice of three different genotypes ($p53^{+/+}$, $p53^{+/-}$, $p53^{-/-}$) (SI Fig. 9*B*), suggesting that p53 is not a major player in this setting. Interestingly, although we were unable to see any p53 expression in the hair bulb throughout hair follicle cycle (data not shown), the levels of

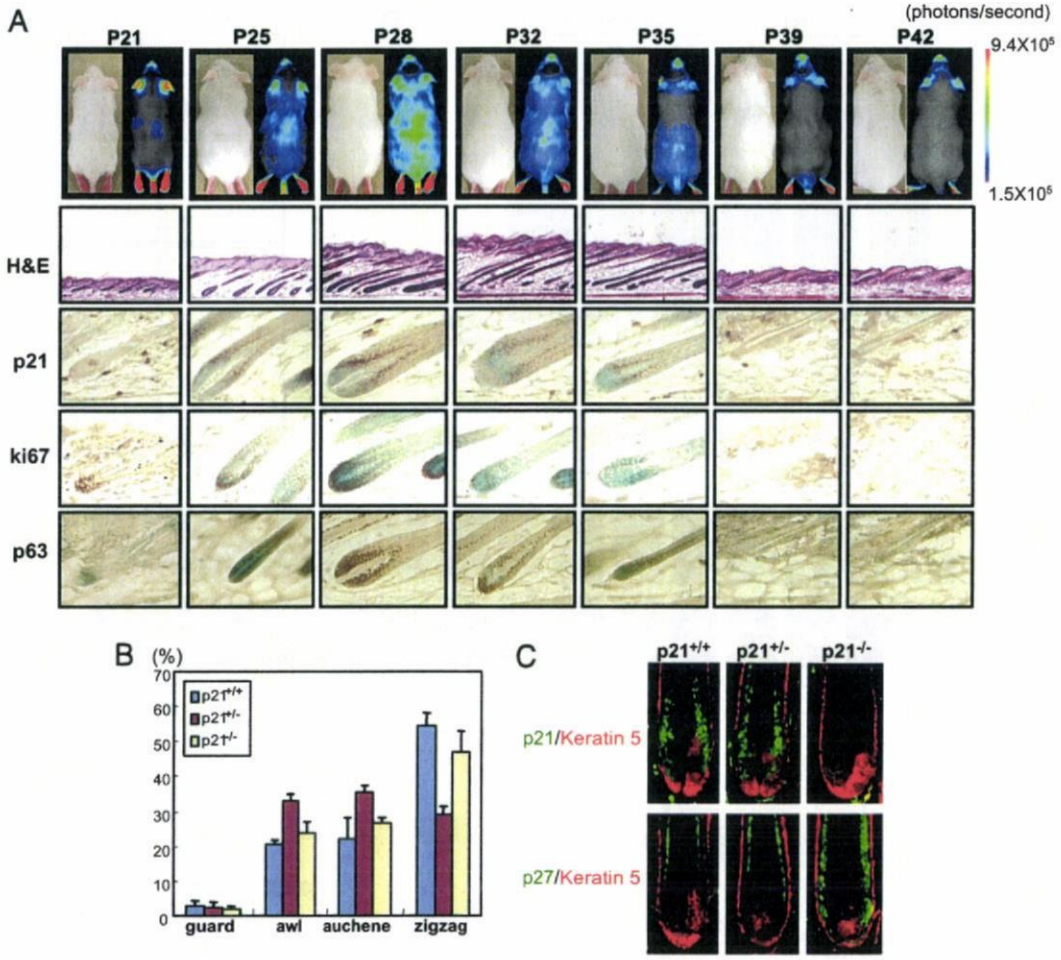


**Fig. 3.** Real-time imaging of hair follicle cycle oscillation in living mice. (*A*) The p21-*p*-luc mice were subjected to noninvasive BLI from postnatal day 21 (P21) to P42. Representative images of five different experiments are shown at the top. The color bar indicates photons with minimum and maximum threshold values. At the indicated time point of postnatal development, dorsal skin of p21-*p*-luc mice was harvested and processed for H&E staining or for immunohistochemistry. (*B*) Summary of the prevalence of hair phenotypes in mice of different $p21^{Waf1/Cip1}$ genotype (C57BL/6 background). The means ± SD of three independent experiments are shown. (*C*) Immunofluorescence of dorsal skin section from P28 mice was performed by using antibodies against $p21^{Waf1/Cip1}$ (green) or $p27^{Kip1}$ (green). Keratin 5 (red) was used as a marker for outer root sheath.

p63 (34), a member of p53-family of transcription factors, were dramatically increased in anagen hair bulbs (Fig. 3*A*). Together, these results imply that p63, but not p53, may play a critical role in the regulation of hair development.

## Discussion

In this study, we generated a transgenic mouse model to visualize $p21^{Waf1/Cip1}$ gene expression in living animals. The p21-*p*-luc mice carry the firefly luciferase cDNA under the control of the $p21^{Waf1/Cip1}$ gene promoter. Because this promoter contains two canonical p53-binding sites, this mouse model is expected to be an ideal system for monitoring not only $p21^{Waf1/Cip1}$ gene expression, but also p53 activation *in vivo*. Indeed, a dramatic induction of bioluminescent signal was observed in various organs within 24 h upon treatment with doxorubicin, a well known DNA-damaging agent that activates p53 (Fig. 1 and SI Fig. 4). Notably, different dynamics of $p21^{Waf1/Cip1}$ gene expression were observed when p21-*p*-luc mice were irradiated with x-ray (SI Fig. 5). In both cases, the levels of bioluminescent signals observed were well correlated with those of endogenous $p21^{Waf1/Cip1}$ mRNA detected by RT-PCR analysis (Fig. 1 and SI Figs. 4 and 5), indicating that the p21-*p*-luc mice provide an ideal tool to monitor the expression of $p21^{Waf1/Cip1}$ gene and/or activity of p53 in living animals. Interestingly, neither doxorubicin nor x-rays induced $p21^{Waf1/Cip1}$ gene expression in the small intestine, implying that p53 is not a major regulator of $p21^{Waf1/Cip1}$ gene expression in the small intestine, as suggested by previous studies (35).

By monitoring and quantifying $p21^{Waf1/Cip1}$ gene expression repeatedly in the same mouse throughout its entire life span, we revealed the dynamics of $p21^{Waf1/Cip1}$ gene expression during the aging process in living mice. Only a slight (3- to 4-fold) induction of bioluminescent signal was observed in kidney, but not in other organs, as mice age (SI Fig. 7). Moreover, strong signs of p53 activation and DNA damage responses were virtually undetectable in aged kidney (SI Fig. 7). These results were unexpected because several lines of evidence suggest that p53-dependent induction of $p21^{Cip1/Waf1}$ is involved in the aging process (22, 23, 36). Our results are, however, consistent with a recent RT-PCR-based study showing that only a slight increase in the $p21^{Waf1/Cip1}$ gene expression was seen in tissues from old mice versus young mice (37, 38). Moreover, it has been shown that increased p53 expression under the endogenous p53 gene promoter protects mice from tumorigenesis without showing any indication of

accelerated aging (39). Furthermore, $p21^{Waf1/Cip1}$ appears to play protective effects on stem cell exhaustion and ionizing radiation, which may underlie the long-term homeostasis throughout entire life span (40–42). Thus, it is likely that the role of $p21^{Waf1/Cip1}$ in organismal aging is context-dependent and more complicated than envisaged.

Another important aspect of the $p53/p21^{Waf1/Cip1}$ pathway is the induction of cellular senescence (4, 24), the state of permanent cell cycle arrest provoked by a variety of oncogenic stimuli including oncogenic *ras* expression in cultured primary cells (43–45). Because this mechanism is poorly understood *in vivo* (46), we tested this notion using our *in vivo* BLI system. Indeed, DMBA/TPA treatment, which causes an oncogenic mutation of the endogenous H-*ras* gene (25, 26), resulted in a significant induction of $p21^{Waf1/Cip1}$ expression accompanied by skin papilloma formation (Fig. 2*A*). Because the induction of $p21^{Waf1/Cip1}$ expression can be seen from the very beginning of papilloma formation and was further enhanced as the papillomas developed (Fig. 2*A*), the $p21^{Waf1/Cip1}$ gene is likely to play multiple roles in preventing benign skin papilloma formation and/or malignant conversion. These results are somewhat consistent with two conflicting reports; one shows that disruption of the $p21^{Waf1/Cip1}$ gene accelerates benign skin papilloma formation but not malignant conversion (27), and the other shows that disruption of the $p21^{Waf1/Cip1}$ gene accelerates malignant conversion but not benign skin papilloma formation (28).

During the time-course BLI experiments in skin tumor formation, we unexpectedly found that the expression of $p21^{Waf1/Cip1}$ oscillates over the 3-week time course of the hair follicle cycle (Figs. 2 *C* and *D* and 3*A*). Moreover, although the morphology of the four main hair types was not remarkably different, the proportion of zigzag hairs, which are produced by the smallest hair bulb, was significantly reduced in $p21^{+/-}$ mice (Fig. 3*B*). Surprisingly, the effects of $p21^{Waf1/Cip1}$ deficiency were less pronounced in $p21^{-/-}$ mice than in heterozygotes (Fig. 3*B*) because of an up-regulation of $p27^{Kip1}$ expression in the hair bulb of $p21^{-/-}$ mice (Fig. 3*C*). In concordance with this notion, recent study revealed that the proportion of zigzag hairs is substantially reduced in mice lacking $p27^{Kip1}$ (33) Thus, there is cross-talk between $p21^{Waf1/Cip1}$ and $p27^{Kip1}$ in controlling hair phenotype. Note that the proportion of zigzag hairs is also reduced in mice lacking the *Sox18* gene (47), and Sox family transcription factors are known to activate $p21^{Waf1/Cip1}$ expression (48). Thus, it is tempting to speculate that Sox18 controls hair phenotype through regulating $p21^{Waf1/Cip1}$ gene expression in the hair bulb. It is also important to note, however, that the expression of p63 (34), a member of p53 family transcription factor, overlapped with that of $p21^{Waf1/Cip1}$ in the hair bulb (Fig. 3*A*). It is therefore likely that $p21^{Waf1/Cip1}$ gene expression is controlled by multiple factors in hair bulbs.

We are currently uncertain about the biological consequence of alteration of the zigzag hair proportion in $p21^{+/-}$ mice. However, because the hair coat plays a crucial role in controlling body temperature in the wild, it is interesting to speculate that $p21^{Waf1/Cip1}$ and/or $p27^{Kip1}$ may be involved in temperature control in the wild. Taken together, our results reveal an unexpected role for $p21^{Waf1/Cip1}$ and provide an insight into how the hair phenotype is determined. Visualizing the dynamics of $p21^{Waf1/Cip1}$ gene expression in living mice, therefore, provides a powerful tool for not only help to resolve and clarify issues connecting *in vitro* studies but also reveals unrecognized functions of this key proliferative regulator in various physiological processes *in vivo*.

## Materials and Methods

**Generation of p21-*p*-luc transgenic mouse.** The 2.5-kb fragment of the $p21^{Waf1/Cip1}$ gene promoter containing two p53-binding sites (GenBank accession number: NW_923073.1; from 9663447 to 9665888) was placed in front of the firefly luciferase reporter cDNA in the pGL3-basic plasmid vector (Promega, Madison, WI) (see plasmid construction map in SI Fig. 10). The plasmid DNA was digested with XhoI and SalI, and the DNA fragment containing the $p21^{Waf1/Cip1}$ gene promoter, luciferase cDNA, and polyA signal was isolated and used for microinjection. The transgenic mouse strain was generated by pronuclear microinjection of the reporter transgene into fertilized CD1 oocytes. Genotyping of transgenic mice was determined by PCR and was confirmed by whole-body BLI. One transgenic line, #34 (CDB0415T-34), was selected for studies described in this article because the levels of bioluminescence signals were well correlated with those of endogenous $p21^{Waf1/Cip1}$ mRNA. All animals were cared for by using protocols approved by the Committee for the Use and Care of Animals of the University of Tokushima.

**Bioluminescence Imaging.** For the detection of luciferase expression, mice were anesthetized, injected i.p. with D-luciferin sodium salt (75 mg/kg) 5 min before beginning photon recording (16–20). Mice were placed in the light-tight chamber, and a gray-scale image of the mice was first recorded with dimmed light, followed by acquisition of luminescence image by using a cooled CCD camera (Princeton Instruments, Trenton, NJ). The signal-to-noise ratio was increased by 2 × 2 binning and 5 min exposure, unless otherwise stated in the text. For colocalization of the luminescent photon emission on the animal body, gray scale and pseudocolor images were merged by using IMAGE-PRO PLUS (Media Cybernetics, Bethesda, MD).

**Tumor-Induction Experiments.** Twelve mice of the p21-*p*-luc line, in the resting phase of the hair cycle (8-week-old), were shaved and treated with 7,12-dimethylbenzanthracene (DMBA) (100 μg in 100 μl of acetone). One week after DMBA treatment, mice were subsequently treated twice a week with TPA (12.5 μg in 100 μl of acetone) for 20 weeks (25, 26). Control mice were treated with acetone instead of DMBA/TPA.

**Semiquantitative RT-PCR.** Total RNA was isolated by using TRIzol reagent (Invitrogen, Carlsbad, CA), and 2 μg of total RNA was used for the reverse-transcriptase reaction. The PCR was performed by using Blend Taq polymerase (TOYOBO, Osaka, Japan) with primers specific for the mouse $p21^{Waf1/Cip1}$ gene and the mouse *β-actin* gene. The PCR primer sequences used are shown in *SI Text*.

**Real-Time RT-PCR.** Quantitative real-time RT-PCR was performed by using the SYBER Premix EX Taq system (TAKARA, Otsu, Japan) and an ABI Prism 7900HT (Applied Biosystems, Foster City, CA). Amplified signals were confirmed to be single bands by gel electrophoresis and were normalized to the levels of GAPDH. Data were analyzed by using SDS2.1 software (Applied Biosystems). The PCR primer sequences used are shown in *SI Text*.

**Histology and Immunohistochemistry.** Biopsies of mouse skin taken from the middorsal region were fixed in 10% formalin for a 24 h or longer, progressively dehydrated through gradients of alcohol, and embedded in paraffin. Samples were sectioned on a microtome (5-μm-thick), deparaffinized in xylene, rehydrated, and then stained with hematoxylin and eosin (H&E). The hair cycle status was determined by histological examination. For antibody staining, deparaffinized and rehydrated sections were exposed to heat-induced antigen retrieval for 5 min or 20 min in 10 mM citrate buffer (pH 6.0). After washing in PBS, endogenous peroxidase activity was quenched for 15 min in 1% $H_2O_2$ in methanol, followed by washing with PBS. The sections were

incubated in blocking serum for 1 h at room temperature. After incubation with primary antibodies overnight at 4°C, biotinylated anti-mouse secondary antibody was applied and detected by the avidin–biotin peroxidase technique using the DAB kit (DAKO, Glostrup, Denmark) and then counterstained with methyl green. For immunofluorescence, the relevant Alexa Fluor 488 goat anti-mouse or 546 goat anti-rabbit antibodies (1:1,000; Invitrogen) were used for detection of primary antibodies. Fluorescence images were observed and photographed by using an immunofluorescence microscope (Carl Zeiss, Oberkochen, Germany). The primary antibodies used are shown in *SI Text*.

**Hair Measurements.** Hair was removed from the middorsal region of each mouse (8-week-old) to reduce the potential regional variation, although this is not known to occur in the dorsal region of the mouse. One hundred hairs were examined to determine the percentage of each hair type.

We thank Dr. P. Leder (Department of Genetics, Harvard Medical School, Boston, MA) for providing $p21^{Waf1/Cip1}$ knockout mice. We also thank Ms. S. Chiba for her assistance in various mouse experiments. This work was supported by grants from Ministry of Education, Science, Sports, and Culture of Japan, the Astellas Foundation for Research on Metabolic Disorders and the Astellas Foundation for Research on Medical Resources.

1. El-Deiry WS, Tokino T, Velculescu VE, Levy DB, Parsons R, Trent JM, Lin D, Mercer WE, Kinzler KW, Vogelstein B (1993) *Cell* 75:817–825.
2. Harper JW, Adami GR, Wei N, Keyomarsi K, Elledge SJ (1993) *Cell* 75:805–816.
3. Xiong Y, Hannon GJ, Zhang H, Casso D, Kobayashi R, Beach D (1993) *Nature* 366:701–704.
4. Noda A, Ning Y, Venable SF, Pereira-Smith OM, Smith JR (1994) *Exp Cell Res* 211:90–98.
5. Sherr CJ, Roberts JM (1999) *Genes Dev* 13:1501–1512.
6. Rowland BD, Peeper DS (2006) *Nat Rev Cancer* 6:11–23.
7. El-Deiry WS (1998) *Curr Top Microbiol Immunol* 227:121–137.
8. Donehower LA, Harvey M, Slagle BL, McArthur MJ, Montgomery CA, Jr, Butel JS, Bradley A (1992) *Nature* 356:215–221.
9. Jacks T, Remington L, Williams BO, Schmitt EM, Halachmi S, Bronson RT, Weinberg RA (1994) *Curr Biol* 4:1–7.
10. Deng C, Zhang P, Harper JW, Elledge SJ, Leder P (1995) *Cell* 82:675–684.
11. Brugarolas J, Chandrasekaran C, Gordon JI, Beach D, Jacks T, Hannon GJ (1995) *Nature* 377:552–557.
12. Sage J, Mulligan GJ, Attardi LD, Miller A, Chen S, Williams B, Theodorou E, Jacks T (2000) *Genes Dev* 14:3037–3050.
13. Ciemerych MA, Kenney AM, Sicinska E, Kalaszczynska I, Bronson RT, Rowitch DH, Gardner H, Sicinski P (2002) *Genes Dev* 16:3277–3289.
14. Contag PR, Olomu IN, Stevenson DK, Contag CH (1998) *Nat Med* 4:245–247.
15. Gross S, Piwnica-Worms D (2005) *Cancer Cell* 7:5–15.
16. Uhrbom L, Nerio E, Holland EC (2004) *Nat Med* 10:1257–1260.
17. Zhang GJ, Safran M, Wei W, Sorensen E, Lassota P, Zhelev N, Neuberg DS, Shapiro G, Kaelin WG, Jr (2004) *Nat Med* 10:643–648.
18. Li F, Sonveaux P, Rabbani ZN, Liu S, Yan B, Huang Q, Vujaskovic Z, Dewhirst MW, Li CY (2007) *Mol Cell* 26:63–74.
19. Vooijs M, Jonkers J, Lyons S, Berns A (2002) *Cancer Res* 62:1862–1867.
20. Paulmurugan R, Umezawa Y, Gambhir SS (2002) *Proc Natl Acad Sci USA* 99:15608–15613.
21. Sharpless NE, DePinho RA (2002) *Cell* 110:9–12.
22. Tyner SD, Venkatachalam S, Choi J, Jones S, Ghebranious N, Igelmann H, Lu X, Soron G, Cooper B, Brayton C, *et al.* (2002) *Nature* 415:45–53.
23. Maier B, Gluba W, Bernier B, Turner T, Mohammad K, Guise T, Sutherland A, Thorner M, Scrable H (2004) *Genes Dev* 18:306–319.
24. Serrano M, Lin AW, McCurrach ME, Beach D, Lowe SW (1997) *Cell* 88:593–602.
25. Quintanilla M, Brown K, Ramsden M, Balmain A (1986) *Nature* 322:78–80.
26. Kemp CJ (2005) *Semin Cancer Biol* 15:460–473.
27. Weinberg WC, Fernandez-Salas E, Morgan DL, Shalizi A, Mirosh E, Stanulis E, Deng C, Hennings H, Yuspa SH (1999) *Cancer Res* 59:2050–2054.
28. Topley GI, Okuyama R, Gonzales JG, Conti C, Dotto GP (1999) *Proc Natl Acad Sci USA* 96:9089–9094.
29. Oskarsson T, Essers MA, Dubois N, Offner S, Dubey C, Roger C, Metzger D, Chambon P, Hummler E, Beard P, Trumpp A (2006) *Genes Dev* 20:2024–2029.
30. Fuchs E (2007) *Nature* 445:834–842.
31. Flores I, Cayuela ML, Blasco MA (2005) *Science* 309:1253–1256.
32. Sarin KY, Cheung P, Gilison D, Lee E, Tennen RI, Wang E, Artandi MK, Oro AE, Artandi SE (2005) *Nature* 436:1048–1052.
33. Sharov AA, Sharova TY, Mardaryev AN, Tommasi di Vignano A, Atoyan R, Weiner L, Yang S, Brissette JL, Dotto GP, Botchkarev VA (2006) *Proc Natl Acad Sci USA* 103:18166–18171.
34. Senoo M, Pinto F, Crum CP, McKeon F (2007) *Cell* 129:523–536.
35. Macleod KF, Sherry N, Hannon G, Beach D, Tokino T, Kinzler K, Vogelstein B, Jacks T (1995) *Genes Dev* 9:935–944.
36. Choudhury AR, Ju Z, Djojosubroto MW, Schienke A, Lechel A, Schaetzlein S, Jiang H, Stepczynska A, Wang C, Buer J, *et al.* (2007) *Nat Genet* 39:99–105.
37. Krishnamurthy J, Torrice C, Ramsey MR, Kovalev GI, Al-Regaiey K, Su L, Sharpless NE (2004) *J Clin Invest* 114:1299–1307.
38. Edwards MG, Anderson RM, Yuan M, Kendziorski CM, Weindruch R, Prolla TA (2007) *BMC Genomics* 8:80.
39. Garcia-Cao I, Garcia-Cao M, Martin-Caballero J, Criado LM, Klatt P, Flores JM, Weill JC, Blasco MA, Serrano M (2002) *EMBO J* 21:6225–6235.
40. Cheng T, Rodrigues N, Shen H, Yang Y, Dombkowski D, Sykes M, Scadden DT (2000) *Science* 287:1804–1808.
41. Kippin TE, Martens DJ, van der Kooy D (2005) *Genes Dev* 19:756–767.
42. Wang YA, Elson A, Leder P (1997) *Proc Natl Acad Sci USA* 94:14590–14595.
43. Gil J, Peters G (2006) *Nat Rev Mol Cell Biol* 7:667–677.
44. Campisi J (2005) *Cell* 120:513–522.
45. Takahashi A, Ohtani N, Yamakoshi K, Iida S, Tahara H, Nakayama K, Nakayama KI, Ide T, Saya H, Hara E (2006) *Nat Cell Biol* 8:1291–1297.
46. Narita M, Lowe SW (2005) *Nat Med* 11:920–922.
47. Pennisi D, Bowles J, Nagy A, Muscat G, Koopman P (2000) *Mol Cell Biol* 20:9331–9336.
48. Panda DK, Miao D, Lefebvre V, Hendy GN, Goltzman D (2001) *J Biol Chem* 276:41229–41236.

nature immunology

# Regulation of Naive T Cell Function By the NF-κB2 Pathway

Naozumi Ishimaru, Hidehiro Kishimoto, Yoshio Hayashi & Jonathan Sprent

Reprinted from *Nature Immunology*, Volume 7, July 2006

nature immunology

# Regulation of naive T cell function by the NF-κB2 pathway

Naozumi Ishimaru[1,2], Hidehiro Kishimoto[3], Yoshio Hayashi[2] & Jonathan Sprent[1,4]

**T cell activation involves the orchestration of several signaling pathways, including that of the 'classical' transcription factor NF-κB components NF-κB1–RelA. The function of the 'nonclassical' NF-κB2–RelB pathway is less clear, although T cells lacking components of this pathway have activation defects. Here we show that mice deficient in NF-κB-inducing kinase have a complex phenotype consisting of immunosuppression mediated by $CD25^{-}Foxp3^{-}$ memory $CD4^{+}$ cells and, in the absence of those cells, hyper-responsive naive $CD4^{+}$ T cells, which caused autoimmune lesions after adoptive transfer into hosts deficient in recombination-activating genes. Biochemical studies indicated involvement of a cell-intrinsic mechanism in which NF-κB2 (p100) limits nuclear translocation of NF-κB1–RelA and thereby functions as a regulatory 'brake' for the activation of naive T cells.**

The transcription factor NF-κB is key in the regulation of many inflammatory processes of immune cells[1]. The NF-κB family consists of five subunits: NF-κB1 (p105-p50), NF-κB2 (p100-p52), RelA (p65), RelB and c-Rel. Hetero- or homodimers of these subunits can be translocated into the nucleus to bind to κB sequences of neighboring 'target' genes, thus regulating the transcription of genes required for cell activation, survival and development[2]. Two pathways of NF-κB have been defined in immune cells[3]: the 'classical' pathway, which is initiated by complexes of NF-κB1 and RelA, and an alternative or 'nonclassical' pathway, which is initiated by complexes of NF-κB2 and RelB.

For T cells, stimulation via the T cell receptor (TCR) and costimulatory molecules such as CD28 leads to NF-κB activation through a variety of intracellular signaling molecules[4]. Initially, TCR-CD28 signaling via many adaptor molecules leads to activation of protein kinase C-θ (PKC-θ)[5]. Thereafter, CARMA1–Bcl-10–MALT1 proteins 'downstream' of PKC-θ activate IκB kinase (IKK) complexes, including IKKα, IKKβ and the adaptor protein IKKγ (also called NEMO)[6,7]. Activated IKK complexes then phosphorylate IκB, releasing it from its constitutively bound state with cytoplasmic NF-κB complexes (mainly NF-κB1–RelA) that normally prevents NF-κB complexes from translocating to the nucleus. Ubiquitination and degradation of IκB by IKK complexes allows components of the classical NF-κB pathway, especially p50-RelA, to be transported into the nucleus, thus promoting transcription of essential target genes required for survival, cytokine and chemokine production, upregulation of adhesion molecules, organogenesis and apoptosis in the immune system[8]. The classical NF-κB pathway is especially important for the synthesis of interleukin 2 (IL-2) as well as IL-2 receptor (IL-2R, also called CD25) in T cells[9,10]. As for the alternative, nonclassical NF-κB pathway, signals from specific cytokine receptors (such as the lymphotoxin-β receptor) activate NF-κB-inducing kinase (NIK) as well as PKC-θ and CARMA1–Bcl-10–MALT1, which in turn activate homodimers of IKKα that are required for the cleavage of p100 to p52 (refs. 11–13). Complexes of p52 and RelB then translocate into the nucleus to regulate transcription of a different set of genes.

Studies of gene-knockout mice have demonstrated that individual members of the NF-κB family have distinct roles *in vivo* in T cell function. Thus, T cell proliferation and T helper type 2 cytokine production is reduced in NF-κB1-deficient ($Nfkb1^{-/-}$) mice, and these mice show increased susceptibility to experimental autoimmune encephalomyelitis, typhlocolitis and infection with *Leishmania major* but are resistant to asthma[14–17]. RelA-deficient ($Rela^{-/-}$) mice have a phenotype that is embryonically lethal, but studies with fetal liver chimeras indicate that $Rela^{-/-}$ T cells are functionally defective[18,19]. RelB-deficient ($Relb^{-/-}$) mice are viable but develop systemic inflammation and severe anemia around 2–3 months of age, and the T cell and B cell functions of these mice are suppressed[20]. NF-κB2-deficient ($Nfkb2^{-/-}$) mice have B cell defects as well as T cell hyperplasia and hyperactivation of dendritic cells[21,22]. Finally, mice deficient in c-Rel ($Rel^{-/-}$) have B cell defects, impaired T cell proliferative responses and reduced susceptibility to experimental autoimmune encephalomyelitis[23,24]. Nevertheless, precise information about the functions of the individual NF-κB family members on T cell function is still unclear.

The importance of NIK for NF-κB activation has been demonstrated in studies of NIK-deficient ($Map3k14^{-/-}$) mice and also mice with alymphoplasia ($Map3k14^{aly/aly}$ or 'aly/aly' mice), which carry a mutation of *Map3k14*. Functionally, NIK is key in regulating the

[1]The Scripps Research Institute, La Jolla, California 92037, USA. [2]Department of Oral Molecular Pathology, Institute of Health Biosciences, Tokushima University Graduate School, Tokushima 770-8504, Japan. [3]Research Institute for Biological Sciences, Tokyo University of Science, Noda-City, Chiba 278-0022, Japan. [4]Garvan Institute of Medical Research, Darlinghurst NSW 2010, Australia. Correspondence should be addressed to J.S. (j.sprent@garvan.org.au).

Received 27 January; accepted 26 April; published online 28 May 2006; doi:10.1038/ni1351

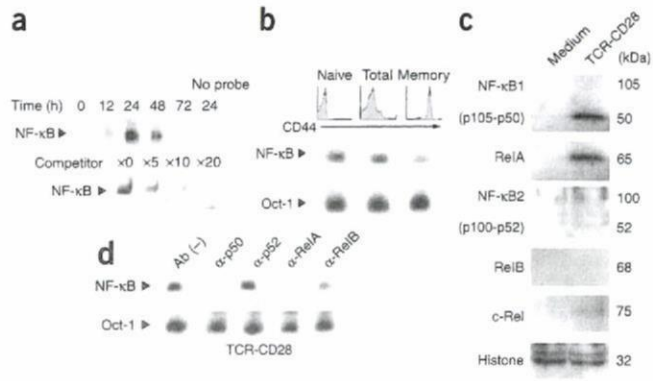


**Figure 1** NF-κB activation in CD4+ T cells. (**a**) EMSA of NF-κB activity in nuclear extracts from CD4+ T cells from lymph nodes of B6 mice stimulated (times, above lanes) with crosslinked anti-TCR (1 μg/ml) and anti-CD28 (20 μg/ml). Below, EMSA with competitor (concentration, above lanes). (**b**) EMSA of NF-κB and Oct-1 activity in nuclear extracts of total, naive CD44$^{lo}$ or memory CD44$^{hi}$ CD4+ T cells stimulated for 24 h by TCR-CD28 ligation as in **a**. Top, CD44 expression on the cells before culture, determined by flow cytometry. (**c**) Immunoblot for NF-κB subunits in nuclear extracts of naive CD4+ T cells cultured in medium alone or activated for 24 h by TCR-CD28 ligation. (**d**) Antibody supershift assay of nuclear extracts from purified naive CD4+ T cells obtained from B6 lymph nodes; cells were stimulated for 24 h by TCR-CD28 ligation. Ab (–), no antibody; α-, antibody to. Results are representative of three to five independent experiments.

processing of p100 to p52 through IKKα both in hematopoietic cells and osteoclasts[25–27]. *Map3k14*$^{-/-}$ and aly/aly mice lack lymph nodes, and, at least for aly/aly mice, T cells show defective proliferation and IL-2 production in response to stimulation with antibody to CD3 (anti-CD3)[13,28,29]. In addition, NIK may be involved in the maintenance of central tolerance in the thymus[30]. Moreover, aly/aly mice as well as *Relb*$^{-/-}$ mice show signs of autoimmune disease[20,31,32]. Despite those findings, the mechanism for the regulation of peripheral T cell activation through NIK has not been established.

Much of the data on the function of NIK has come from studies of T cell populations that have not been separated into individual subsets based on their activation status. Expression of certain surface markers, notably CD44, distinguishes mature T cells as those that are immunologically naive (naive T cells) versus those that have been primed through contact with environmental antigens (memory T cells)[33,34]. In mice, low or intermediate expression of CD44 (CD44$^{lo}$ or CD44$^{int}$) indicates a naive differentiation status, whereas CD44$^{hi}$ cells have differentiated into memory cells. Here we examine the functions of NIK, both *in vivo* and *in vitro*, in purified subsets of naive and memory CD4+ cells.

## RESULTS

### NF-κB1 in CD4+ cell activation

To define the kinetics of NF-κB activation during the course of normal T cell activation, we analyzed the transcriptional activity of NF-κB in stimulated CD4+ T cells from normal C57BL/6 (B6) mice by electrophoretic mobility-shift assay (EMSA) using an NF-κB-binding DNA probe. After total CD4+ T cells were stimulated with plate-bound monoclonal antibodies (mAbs) to TCR and CD28, activation of NF-κB, measured in nuclear extracts of the cells, reached a peak after 24 h and then decreased to undetectable amounts by 72 h (**Fig. 1a**). We confirmed the specificity of NF-κB activation by using unlabeled NF-κB-binding DNA as a competitor to diminish the signal.

To determine NF-κB activation in naive and memory CD4+ T cells, we stimulated enriched subsets of normal B6 CD44$^{lo}$ (naive) and CD44$^{hi}$ (memory) CD4+ T cells by TCR-CD28 ligation for 24 h, followed by EMSA to detect transcriptional activity of NF-κB in the nuclear extracts; we used total CD4+ cells as a control. Nuclear translocation of NF-κB was much more prominent for naive CD4+ cells than for memory cells; in contrast, transcriptional activity of an internal control (Oct-1) was the same for both subsets of CD4+ T cells (**Fig. 1b**).

To determine the extent of nuclear translocation of individual NF-κB family members in each subset, we treated naive CD4+ T cells for 24 h with mAbs to TCR and CD28, then purified nuclear extracts and did immunoblot analysis with NF-κB protein subunit–specific antibodies. Nuclear extracts had substantial amounts of both p50 and RelA, a small amount of c-Rel protein and a conspicuous absence of p52 or RelB proteins (**Fig. 1c**). Consistent with those findings, analysis of the nuclear extracts after incubation with antibodies specific for each NF-κB protein subunit ('supershift assay') showed that the mobility shift of the NF-κB DNA probe was greatest with anti-p50 or anti-RelA but only minimal with anti-p52 or anti-RelB (**Fig. 1d**), suggesting a predominance of p50-RelA dimers. That indicated, therefore, that early activation of NF-κB in naive CD4+ cells reflects nuclear translocation of NF-κB1 (p50)–RelA, with little or no contribution from NF-κB2 (p52)–RelB.

### NF-κB2 in CD4+ T cell activation

The findings reported above failed to explain the T cell defects seen in NIK-deficient aly/aly and *Relb*$^{-/-}$ mice[13,20,29]. Total CD4+ T cells have been used in studies published before; thus, it was unclear whether the abnormalities noted occur at the level of specific CD4+ T cell subsets. To examine that issue, we compared the functions of total CD4+ cells and enriched subsets of naive and memory CD4+ cells. As anticipated from prior studies[13,20,29], the proliferative responses of total CD4+ cells treated for 3 d *in vitro* with mAbs to TCR and CD28 were much lower (50–70% reduction) for *Relb*$^{-/-}$, aly/aly and *Map3k14*$^{-/-}$ mice than for heterozygous littermates or wild-type B6 mice (**Fig. 2a**). We obtained similar findings with mixed-lymphocyte reactions, in which proliferative responses were elicited by exposure to allogeneic (BALB/c) spleen cells (**Fig. 2b**). The decreased response of *Relb*$^{-/-}$, aly/aly and *Map3k14*$^{-/-}$ CD4+ cells was only mildly improved after removal of CD25+CD4+cells; that is, cells with T regulatory function ($T_{reg}$ cells)[35–37] (**Fig. 2a–c**). That finding was unexpected because removing CD25+ $T_{reg}$ cells from control CD4+ cell samples, thus leaving CD25−CD4+ cells, led to enhanced responses (**Fig. 2c**, left versus right). Notably, CD25+CD4+ cells are nearly all CD44$^{hi}$, but about 50% of CD44$^{hi}$ cells are CD25−. In wild-type mice, CD25−CD44$^{hi}$CD4+ cells have little or no T regulatory function and are generally considered to be memory (or 'memory-phenotype') cells. As shown for aly/+ cells in **Figure 2c**, left, depleting normal control cell samples of both CD25+ and CD44$^{hi}$ cells, thus leaving enriched naive CD25−CD44$^{lo}$CD4+ cells, led to much lower proliferative responses than those noted after removal of CD25+ cells alone. These findings indicated that in wild-type mice, total CD44$^{hi}$ cells are a mixture of two functionally distinct populations: an inhibitory population of CD25+ $T_{reg}$ cells, and a helper population of CD25− T memory cells, which probably release stimulatory cytokines (discussed below). The situation with respect to these cell subtypes and functions is radically different for NIK-deficient cells.

For NIK-deficient aly/aly cells, poor TCR-mediated proliferative responses were generally improved only slightly after selective removal

of $CD25^+$ cells (classical $T_{reg}$ cells). In contrast, removal of both $CD25^+$ and $CD44^{hi}$ cells led to a substantial increase in the response; thus, the remaining $CD25^-CD44^{lo}CD4^+$ naive aly/aly T cells demonstrated a hyper-responsive proliferation compared with that of a comparable population of $CD4^+$ cells from control mice (**Fig. 2a,b,d** versus **Fig. 2d–f**). We noted the hyper-responsiveness of $CD44^{lo}CD4^+$ aly/aly cells in samples from *Map3k14*$^{-/-}$ and *Relb*$^{-/-}$ mice, and it was apparent for both mixed-lymphocyte reactions and TCR-CD28–induced proliferation (**Supplementary Fig. 1** online). We also noted hyper-responsiveness for the main subset of $CD44^{int}$ cells, which like $CD44^{lo}$ cells are considered immunologically naive (that is, they have not experienced foreign antigen stimulation; **Fig. 2f**); in contrast, $CD44^{hi}CD4^+$ cells were hypo-responsive compared with control cells (**Fig. 2g** and **Supplementary Fig. 1**). In these and all subsequent experiments, samples were enriched for 'memory' $CD44^{hi}$ cells by removal of $CD25^+$ cells (which included activated T cells as well as $T_{reg}$ cells) and $CD62L^+$ cells.

The main conclusion from the experiments reported above is that in contrast to wild-type control cells, naive $CD4^+$ cells in NIK-deficient and *Relb*$^{-/-}$ mice are poised to hyper-respond to TCR-mediated signals and the hyper-proliferative response is 'suppressed' by $CD25^-CD44^{hi}$ memory T cells (called '$CD44^{hi}CD4^+$ memory T cells' here) when total $CD4^+$ T cells are assayed. As discussed below, the properties of $CD44^{hi}CD4^+$ memory T cells in wild-type and aly/aly mice are very different: $CD44^{hi}CD4^+$ memory T cells from wild-type mice function as helper T cells for primed naive cells, whereas $CD44^{hi}CD4^+$ memory T cells from aly/aly mice function as 'suppressor' cells.

To quantitatively evaluate the suppressor function of aly/aly $CD44^{hi}CD4^+$ memory T cells, we monitored the dilution of carboxyfluorescein diacetate succinimidyl diester (CFSE) in naive $CD44^{lo}CD4^+$ 'reporter' cells preincubated with the fluorescent dye. Early (48 h) proliferative responses of CFSE-labeled control (aly/+) $CD44^{lo}CD4^+$ cells were appreciably enhanced by the addition of a similar number ($5 \times 10^4$) of syngeneic aly/+ $CD44^{hi}CD4^+$ memory T cells (**Supplementary Fig. 2** online). In contrast, the proliferation of aly/aly $CD44^{lo}CD4^+$ cells was reduced considerably by the addition of syngeneic aly/aly $CD44^{hi}CD4^+$ memory T cells (**Supplementary Fig. 2**). We obtained similar results when we incubated $CD44^{hi}CD4^+$ memory T cells from wild-type B6 or aly/aly mice (both Thy-$1.2^+$) with CFSE-labeled $CD44^{lo}CD4^+$ cells from B6.PL mice (Thy-$1.1^+$; **Supplementary Fig. 2**). For $CD44^{hi}CD4^+$ memory T cells from wild-type mice, the 'helper' effect of these cells correlated with increased IL-2 in the mixed cultures (**Supplementary Fig. 2**), presumably reflecting IL-2 synthesis by the added $CD44^{hi}CD4^+$ memory T cells. In contrast, the inhibitory influence of aly/aly $CD44^{hi}CD4^+$ memory T cells correlated with a decrease in IL-2 in the cultures (**Supplementary Fig. 2**). To directly test the function of IL-2 in this experimental situation, we added exogenous IL-2 and found that it was sufficient to overcome the inhibitory effect of adding aly/aly $CD44^{hi}CD4^+$ memory T cells (**Supplementary Fig. 2**).

Because the $CD44^{hi}CD4^+$ memory T cell samples in the experiments reported above were depleted of typical $CD25^+$ $T_{reg}$ cells, the substantial suppressive influence of aly/aly $CD25^-CD44^{hi}CD4^+$ memory T cells was very unexpected. These cells could have had high expression of Foxp3, a transcription factor that in normal mice is selectively expressed mainly in $CD25^+$ $T_{reg}$ cells[38–40]. That was not the case, however, as we found that Foxp3 protein was undetectable in both wild-type and aly/aly $CD25^-CD44^{hi}CD4^+$ memory T cells even after TCR stimulation (**Supplementary Fig. 3** online). Detection of Foxp3 protein was restricted to $CD25^+CD4^+$ typical $T_{reg}$ cells, and the numbers of $Foxp3^+$ cells were much lower (70–80% reduction) for aly/aly than for wild-type, consistent with published findings[30,41].

## Mechanism of suppression

The findings reported above indicated that aly/aly naive and memory T cell subsets differ considerably in their capacity to synthesize and/or use IL-2. To test that hypothesis, we evaluated both cell subsets for IL-2 synthesis and IL-2Rα (CD25) expression after TCR-CD28 ligation (**Fig. 3**). For naive $CD4^+$ T cells, there was somewhat less IL-2, as measured by enzyme-linked immunosorbent assay (ELISA), in the

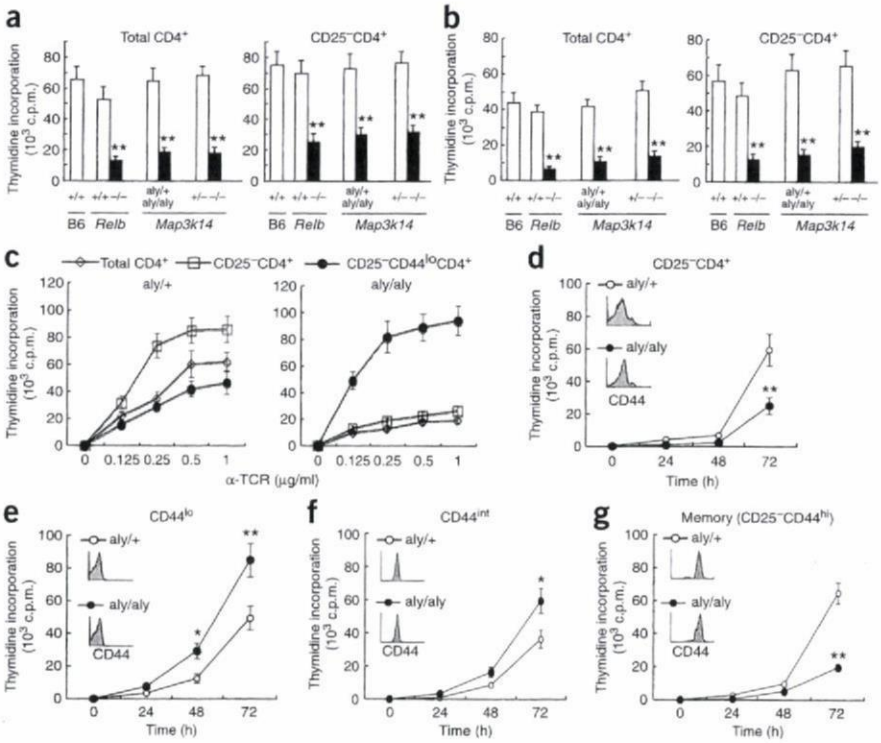


**Figure 2** T cell responses of mice deficient in NF-κB2–RelB. (**a**,**b**) Proliferation assays of total $CD4^+$ and enriched $CD25^-CD4^+$ cell populations from spleens of *Relb*$^{-/-}$, aly/aly, NIK-deficient (*Map3k14*$^{-/-}$) and control (B6, *Relb*$^{+/-}$, aly/+ and *Map3k14*$^{+/-}$) mice stimulated for 72 h by TCR-CD28 ligation as in **Figure 1** (**a**) or by culture for 96 h together with irradiated T cell–depleted spleen cell samples from BALB/c mice (**b**). (**c**) Proliferation assays of total, $CD25^-$ and $CD25^-CD44^{lo}$ $CD4^+$ T cells from aly/+ and aly/aly mice; cells were stimulated for 72 h with 0–1 μg/ml (horizontal axes) of mAb to TCR (α-TCR) and 20 μg/ml of mAb to CD28. (**d**–**g**) Proliferation assays of $CD25^-CD4^+$ cells and enriched subsets of $CD44^{lo}$, $CD44^{int}$ and $CD44^{hi}$ $CD4^+$ T cells (all $CD25^-$) separated by FACSsort and stimulated for 72 h with TCR-CD28 ligation. Insets, CD44 expression on the cells before culture. *, $P < 0.05$, and **, $P < 0.005$, aly/aly mice versus control mice. Data are means ± s.d. of triplicate samples and are representative of three independent experiments.

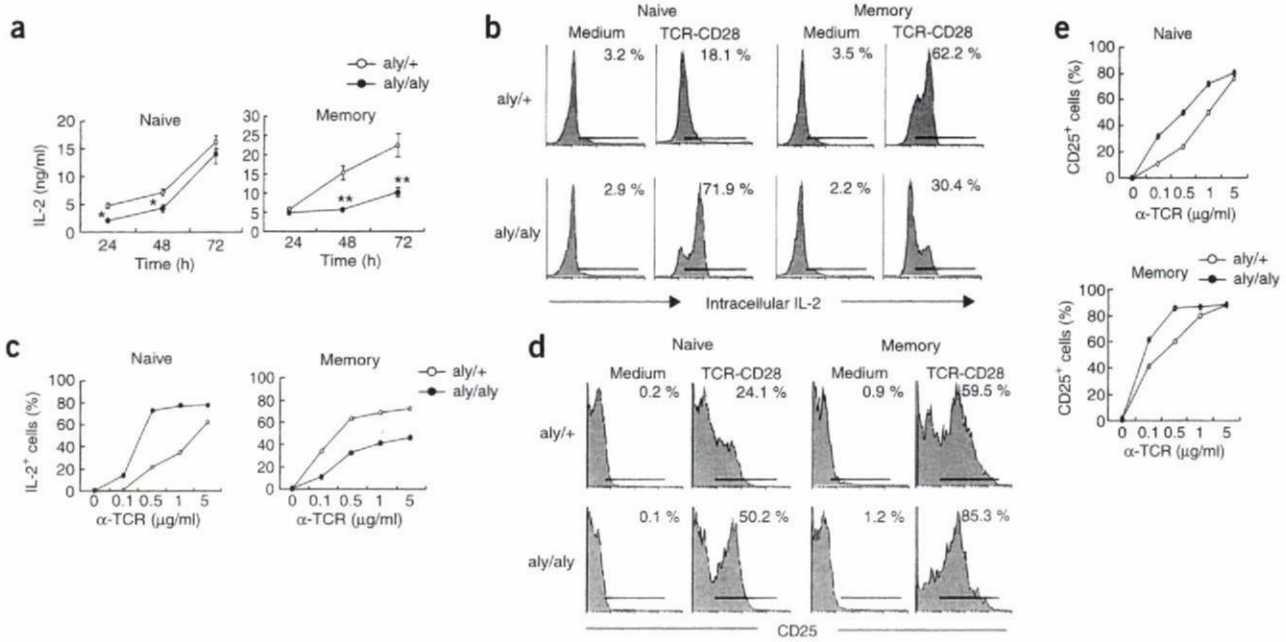


**Figure 3** IL-2 secretion and IL-2R synthesis by aly/aly CD4+ subsets. (**a**) ELISA of IL-2 in culture supernatants of aly/aly and aly/+ naive CD44$^{lo}$ and memory CD44$^{hi}$CD4+ T cells stimulated (time, horizontal axes) by TCR-CD28 ligation (as in **Fig. 1a**). Data are means ± s.d. of triplicate samples and are representative of four independent experiments. *, $P < 0.05$, and **, $P < 0.005$, aly/aly mice versus control mice. (**b**,**c**) Flow cytometry for intracellular IL-2 in aly/aly and aly/+ naive CD44$^{lo}$ and memory CD44$^{hi}$CD4+ T cells stimulated for 24 h with mAb to TCR (0.1–5 μg/ml; horizontal axes) and mAb to CD28 (20 μg/ml; 'TCR-CD28'). (**b**) Representative data for percent IL-2+ cells (numbers above horizontal lines, in top right corners) after stimulation at 0.5 μg/ml of mAb TCR. (**c**) Mean percent of IL-2+ cells after stimulation with 'graded' concentrations of mAb to TCR. (**d**,**e**) Flow cytometry for CD25 expression on CD4+ T cells of aly/aly and aly/+ mice from **b**,**c**. (**d**) Numbers above horizontal lines indicate percent CD25+ cells after stimulation at 0.5 μg/ml of mAb TCR. (**e**) Percent CD25+ cells after stimulation with 'graded' concentrations of mAb to TCR. Results are representative of three to five independent experiments.

culture supernatants of aly/aly cells than of wild-type (aly/+) cells (**Fig. 3a**). That result was unexpected given the enhanced proliferative responses of naive aly/aly cells; however, intracellular staining showed that there was much more IL-2 protein in the cytoplasm of aly/aly cells than wild-type cells (**Fig. 3b**,**c**). Likewise, induction of CD25 cell surface expression was much greater on aly/aly cells than on wild-type cells (**Fig. 3d**,**e**). Hence, the reduced IL-2 in the culture supernatants of naive aly/aly cells presumably reflected enhanced IL-2 consumption through binding to the increased CD25 expressed on the cell surface. From these results we concluded that the increased proliferative responses of aly/aly naive cells correlated with increased IL-2 and IL-2R protein synthesis.

For CD44$^{hi}$CD4+ memory T cells, there was much less IL-2 synthesis in cells from aly/aly mice than in cells from control (aly/+) mice, as assessed by both the amount of IL-2 secreted into the culture supernatant (**Fig. 3a**) and the amount detected inside the cells by intracellular staining (**Fig. 3b**,**c**). However, the results were very different for IL-2R; compared with wild-type CD44$^{hi}$CD4+ memory T cells, aly/aly CD44$^{hi}$CD4+ memory T cells had enhanced CD25 cell surface expression, similar to that seen in the aly/aly naive cells (**Fig. 3d**,**e**), and the cells also demonstrated enhanced CD69 expression (data not shown). Hence, the reduced proliferative response of aly/aly CD44$^{hi}$CD4+ memory T cells correlated with poor IL-2 synthesis despite high IL-2R induction. The suppressive effect of aly/aly CD44$^{hi}$CD4+ memory T cells on naive CD4+ T cells therefore might reflect the possibility that aly/aly CD44$^{hi}$CD4+ memory T cells deplete the cultures of IL-2 because of enhanced expression of CD25. In agreement with that interpretation, proliferative responses of both wild-type and aly/aly naive CD4+ cells were considerably reduced by depleting the cultures of IL-2 with mAb to IL-2 (**Supplementary Fig. 2**). Moreover, in mixed cultures of naive and memory CD4+ T cells (**Supplementary Fig. 2**), poor IL-2 synthesis by these cells combined with high IL-2R expression led to IL-2 depletion, which is the likely mechanistic explanation of the suppressive property of aly/aly memory cells.

The finding that total aly/aly CD4+ cells were hyporesponsive to TCR-CD28 ligation after selective depletion of CD25+ cells suggested that the CD25+ $T_{reg}$ cells in aly/aly mice are functionally defective. Alternatively, the aly/aly $T_{reg}$ cells might have 'normal' suppressive activity but function poorly because their relative numbers are much lower than those in wild-type mice (**Supplementary Fig. 3**). In support of the last idea, the capacity of purified CD25+CD4+ cells to suppress proliferation of wild-type naive CD4+ T cells was almost as efficient for aly/aly CD25+ cells as it was for wild-type CD25+ cells (**Supplementary Fig. 4** online). Likewise, aly/aly and wild-type CD25+ cells were comparable in their low synthesis of IL-2 but high synthesis of both IL-10 and transforming growth factor-β (**Supplementary Fig. 4**).

### *In vivo* responses

To examine responses *in vivo*, we first compared normal and aly/aly CD4+ subsets for their capacity to undergo homeostatic proliferation in syngeneic irradiated mice. As described before[42], the paucity of T cells in irradiated mice allows adoptively transferred CD4+ T cells to proliferate in response to major histocompatibility complex class II–restricted self peptides. Homeostatic proliferation of CFSE-labeled naive CD44$^{lo}$CD4+ cells was greater for aly/aly cells than for normal aly/+ cells (**Fig. 4a**). In contrast, homeostatic proliferation

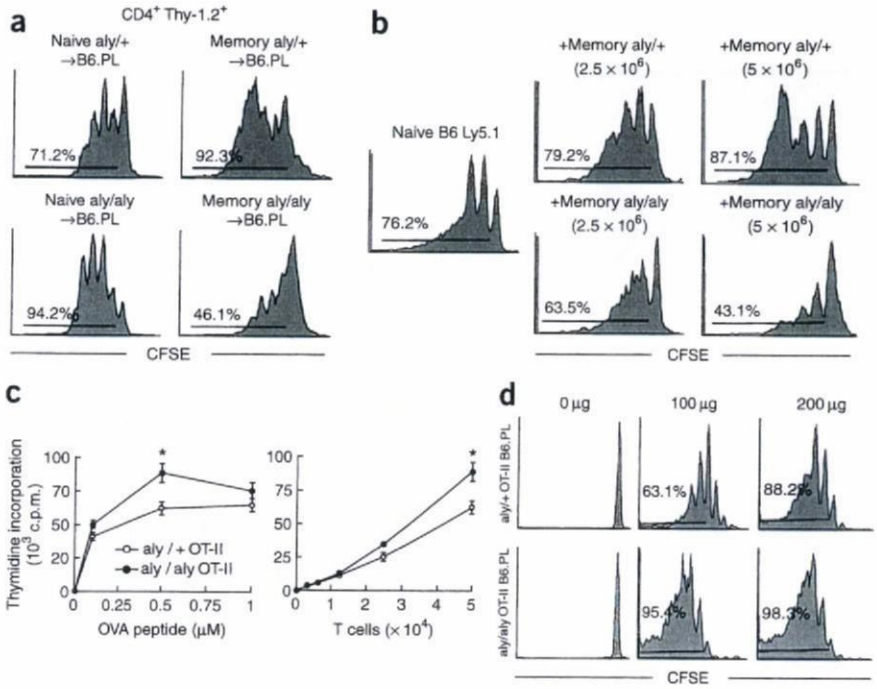


**Figure 4** Proliferative responses of naive and memory aly/aly CD4+ subsets *in vivo*. (**a**) Flow cytometry of CFSE-labeled naive CD44$^{lo}$ or memory CD44$^{hi}$ CD4+ T cells ($5 \times 10^6$) from aly/aly and aly/+ mice (both Thy-1.2) transferred 7 d previously into irradiated (700 rads) B6.PL (Thy-1.1) mice. (**b**) Flow cytometry of CFSE-labeled naive CD4+ T cells ($5 \times 10^6$) from B6 Ly5.1 mice transferred together with unlabeled aly/+ or aly/aly memory cells ($2.5 \times 10^6$ or $5 \times 10^6$; both Ly5.2) into irradiated (700 rads) B6 mice. Ly5.1+CD4+ T splenocytes were evaluated 7 d after transfer. (**c**) Proliferative assay of naive CD44$^{lo}$CD4+ T cells from either aly/aly OT-II or aly/+ OT-II mice cultured for 72 h *in vitro* with irradiated (1,500 cGy) T cell–depleted B6 spleen cell samples ($5 \times 10^5$ cells) in the presence of 'graded' concentrations of OVA peptide (left) or with 'graded' numbers of T cells and 0.5 μM OVA peptide (right). Data are means ± s.d. of triplicate cultures. *, $P < 0.05$, aly/aly OT-II versus aly/+ OT-II cells. (**d**) Flow cytometry of CSFE-labeled naive CD4+ T cells ($5 \times 10^6$) from aly/aly or aly/+ OT-II B6.PL mice (both Thy-1.1+) transferred intravenously into B6 (Thy-1.2+) mice; 1 d later, OVA peptide (0–200 μg) was injected intraperitoneally into recipient mice. Thy-1.1+Vβ5.2+CD4+ T splenocytes were analyzed 3 d after peptide injection. Numbers above horizontal lines (**a**,**b**,**d**) indicate percentages of divided cells from the fourth division. Results are representative of two (**b**) or three (**a**,**c**,**d**) independent experiments.

of CD44$^{hi}$CD4+ memory T cells was much less for aly/aly cells than for normal aly/+ cells. Likewise, homeostatic proliferation of wild-type naive CD4+ cells (CFSE labeled) *in vivo* was enhanced by the addition of wild-type memory CD4+ cells (not CFSE labeled) but was inhibited by the addition of aly/aly CD44$^{hi}$CD4+ memory T cells (**Fig. 4b**). There was also hyper-responsiveness of naive aly/aly CD4+ cells *in vivo* for antigen-specific CD4+ cells. Thus, compared with control aly/+ naive OT-II cells, aly/aly naive CD44$^{lo}$CD4+ OT-II cells demonstrated enhanced proliferative responses to stimulation with specific ovalbumin (OVA) peptide *in vitro* (**Fig. 4c**) and to a limiting dose of OVA peptide (100 μg/mouse) *in vivo* (**Fig. 4d**).

### NF-κB expression in naive versus memory CD4+ cells

To understand the hyper-responsiveness of naive aly/aly cells, it was important to determine the expression of individual NF-κB subunits in wild-type and NIK-deficient CD4+ cells. For naive CD44$^{lo}$CD4+ cells from control aly/+ mice, confocal microscopy after TCR-CD28 ligation for 24 h showed increased synthesis of NF-κB1 and RelA in the cytoplasm and translocation of both subunits to the nucleus (**Fig. 5a**); the two subunits were in close proximity, as indicated by their merged fluorescence. We obtained similar results for naive aly/aly cells, although in this case the fluorescence of NF-κB1 and RelA was stronger in the nucleus than in the cytoplasm, suggesting increased nuclear translocation (**Fig. 5a**). In support of that conclusion, immunoblot analysis of nuclear extracts showed substantially more p50 and RelA in aly/aly cells than in aly/+ cells (**Fig. 5b**). In contrast, NF-κB2 and RelB were almost undetectable in the nuclei of both aly/aly and aly/+ cells, despite high expression of both proteins in the cytoplasm of aly/+ cells (**Fig. 5a**). These data confirmed that at 1 d after TCR-CD28 ligation, nuclear translocation of NF-κB was restricted mainly to NF-κB1 (p50)–RelA dimers (**Fig. 1**). There was also enhanced nuclear translocation of p50 and RelA in naive *Relb*$^{-/-}$ cells, as demonstrated by both confocal and immunoblot analyses (**Supplementary Fig. 5** online). Thus, hyper-responsiveness of naive aly/aly and *Relb*$^{-/-}$ CD4+ T cells correlated with increased nuclear translocation of NF-κB1 (p50)–RelA compared with that of wild-type naive T cells.

Through IκB-like ankyrin repeats, NF-κB2 p100 can bind other NF-κB family members and thereby prevent their nuclear translocation[3]. The hyper-responsiveness of naive aly/aly CD4+ cells, therefore, might reflect reduced p100. To test that possibility, we evaluated cytoplasmic and total cell lysates of naive aly/aly CD4+ cells; both showed a substantial reduction in p100 protein relative to that in aly/+ cells (**Fig. 5c**). We confirmed that result by fluorescence resonance energy transfer (FRET) analysis, which showed that association of p52-p100 with RelA or p50 in aly/aly cells was undetectable (**Fig. 5d**). In contrast, control naive aly/+ cells showed substantial intracytoplasmic association of p52-p100 with both RelA and p50 (**Fig. 5d**). For the control aly/+ and wild-type B6 cells, we confirmed the association of RelA and p50 with p52-p100 by immunoprecipitation of cytoplasmic extracts with anti–p52-p100 followed by immunoblot with NF-κB subunit–specific antibodies. After TCR-CD28 stimulation, p52-p100 protein (mostly p100) was associated with RelB, RelA and p50 but not with c-Rel (**Fig. 5e** and **Supplementary Fig. 5**). Also, immunoprecipitation of [$^{35}$S]methionine-labeled cells with anti-RelA demonstrated a notable p100-RelA complex in wild-type cells but not in aly/aly cells (**Supplementary Fig. 5**). Based on those observations, the hyper-responsiveness of naive aly/aly CD4+ cells can be attributed to reduced p100, which enhances nuclear translocation of p50-RelA and NF-κB-mediated gene transcription and cell activation.

For aly/+ CD44$^{hi}$CD4+ memory T cells, there was increased production and nuclear translocation of both NF-κB1 and RelA after TCR-CD28 ligation, although less than for naive aly/+ cells (**Fig. 5a**). Nuclear translocation of the alternative NF-κB2 and RelB proteins was very prominent for aly/+ CD44$^{hi}$CD4+ memory T cells and correlated with much more p52 in total cell lysates (**Fig. 5c**). In notable contrast, aly/aly CD44$^{hi}$CD4+ memory

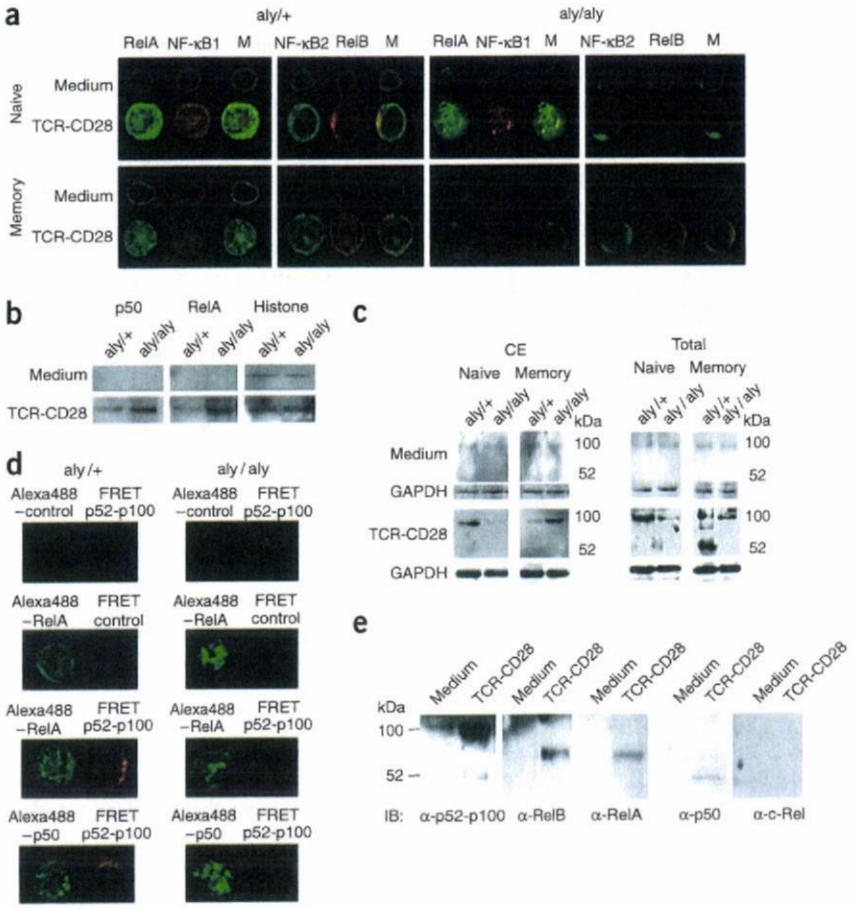


**Figure 5** Molecular interactions between NF-κB subunits during T cell activation. (**a**) Confocal microscopy of naive CD44$^{lo}$ and memory CD4$^+$ T cells from aly/aly and aly/+ mice stimulated for 24 h with TCR-CD28 ligation (as in **Fig. 1**), fixed in 3% paraformaldehyde on a glass slide and stained with anti-p50, anti-RelA, anti-p52 and anti-RelB followed by Alexa Fluor 488–labeled (green) or Alexa Fluor 568–labeled (red) anti-mouse or anti-rabbit IgG. M, merged image. Original magnification, ×630. (**b**) Immunoblot to detect p50 and RelA in nuclear extracts from naive aly/aly and aly/+ CD4$^+$ T cells after 24 h of TCR-CD28 ligation. Histone serves as a control. (**c**) Immunoblot to detect NF-κB2 (p52-p100) in total and cytosolic extracts (CE) of stimulated naive and memory CD4$^+$ T cells from aly/aly and aly/+ mice. Glyceraldehyde phosphate dehydrogenase (GAPDH) serves as a control. (**d**) FRET analysis of aly/aly and aly/+ naive CD4$^+$ T cells stimulated for 24 h with TCR-CD28 ligation, fixed in 3% paraformaldehyde on a glass slide and stained with Alexa Fluor 488–labeled (Alexa488) anti-p50 or anti-RelA and Alexa Fluor 546–labeled anti-p52. The binding of p52 to RelA or p50 is detected as a FRET signal (red). Control, no first antibody. Original magnification, ×630. (**e**) Immunoprecipitation with anti-NF-κB2 p100-p52 and immunoblot (IB) for p100-p52, RelB, p50, RelA and c-Rel in cytosolic extracts of naive B6 CD4$^+$ T cells stimulated for 24 h with TCR-CD28 ligation. Results are representative of three to five independent experiments.

T cells demonstrated no detectable nuclear translocation of RelA, NF-κB1, NF-κB2 or RelB (**Fig. 5a**). For NF-κB2, p100 was apparent in the cytoplasm of aly/aly CD44$^{hi}$CD4$^+$ memory T cells, as shown by both confocal microscopy (**Fig. 5a**) and immunoblot of cytoplasmic extracts (**Fig. 5c**); processing of p100 to p52 was undetectable.

### Kinetics of p100 synthesis and p52 nuclear translocation

The data reported above apply to early (day-1) responses to TCR-CD28. For naive aly/aly CD4$^+$ cells, kinetics experiments showed that p100 in protein cytoplasmic extracts was undetectable for up to 72 h, which correlated with above-normal nuclear translocation of NF-κB1–p50 throughout this time (**Fig. 6a,b**). In contrast, for aly/+ naive CD4$^+$ cells, the amount of p100 in cytoplasmic extracts was high at 24 and 48 h, which correlated with only moderate amounts of NF-κB1–p50 in nuclear extracts. We also noted that nuclear p50 in aly/+ naive cells fell to undetectable amounts by 72 h and was 'replaced' by low but detectable amounts of p52-RelB. We noted the delayed nuclear translocation of p52-RelB only for aly/+ and not aly/aly cells, and this paralleled a decrease in cytoplasmic p100, perhaps reflecting p100-to-p52 processing; delayed nuclear translocation of p52-RelB in aly/+ cells was also apparent by confocal microscopy (**Fig. 6c**). These observations strengthen the view that via direct protein-protein interaction, p100 in the cytoplasm serves to inhibit nuclear translocation of p50-RelA in aly/+ naive CD4$^+$ cells and thereby acts as a 'brake' for gene transcription. The data also indicate that after several days, NF-κB activation in aly/+ naive CD4$^+$ cells involves a 'switch' from NF-κB1- to NF-κB2-dependent pathways.

### Induction of autoimmune disease

NIK-deficient and *Relb*$^{-/-}$ mice develop CD4-dependent, slow-onset (>14 weeks), multiorgan autoimmune disease, which can be 'adoptively transferred' to hosts deficient in recombination-activating gene 2 (*Rag2*$^{-/-}$ hosts)[20,31,32]. Given the data reported above, autoimmune disease might be enhanced by the removal of CD44$^{hi}$CD4$^+$ memory T cells. To investigate that possibility, we adoptively transferred enriched subsets of aly/+ and aly/aly CD4$^+$ T cells into *Rag2*$^{-/-}$ hosts. For both control naive and memory aly/+ CD4$^+$ T cells, cell numbers recovered from the spleen after adoptive transfer were modest (about $5 \times 10^5$ cells/mouse; **Fig. 7a**), infiltration of lymphocytes in the lungs and lacrimal glands was minimal (**Fig. 7b**) and evidence of autoimmune disease in those tissues was undetectable (**Fig. 7c**). We obtained very different results after injecting aly/aly CD4$^+$ cells. For those, injection of either total CD4$^+$ or CD25$^-$CD4$^+$ cells resulted in relatively low recovery of cells from the spleen (**Fig. 7c**), thus correlating with the hyporesponsiveness of the aly/aly cells (as demonstrated above). As for autoimmune disease induction, both populations produced mild but detectable lymphocyte infiltration of lungs and lacrimal glands, with such pathology being slightly more prominent with CD25$^-$ cells (**Fig. 7b,c**). The effects were much more prominent, however, after injection of enriched naive CD4$^+$ cells (that is, samples depleted of both $T_{reg}$ cells and memory CD4$^+$ T cells): cell recoveries were considerably enhanced in the spleen (presumably reflecting enhanced homeostatic proliferation) and there was substantial lymphocytic infiltration and prominent pathology in lung and lacrimal glands. These results demonstrated that the hyper-responsiveness of purified naive aly/aly CD4$^+$ cells applies not only to short-term proliferative

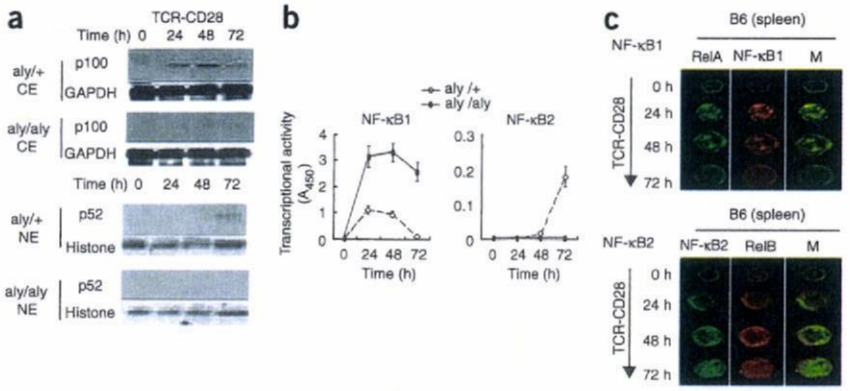


**Figure 6** Kinetics of NF-κB1 and NF-κB2 expression in naive CD4+ cells after TCR ligation. (**a**) Immunoblot to detect p100 and p52 in cytosolic extracts (CE) and nuclear extracts (NE) of aly/+ and aly/aly naive CD4+ cells after 0–72 h of TCR-CD28 ligation. GAPDH and histone serve as controls. Results are representative of two independent experiments. (**b**) Nuclear expression of NF-κB1 and NF-κB2. Relative activities were measured with the nuclear extracts of naive T cells from aly/+ and aly/aly mice stimulated for 0–72 h with TCR-CD28 ligation. Data represent means ± s.d. of triplicate wells. (**c**) Confocal analysis of NF-κB subunits in naive CD4+ cells from B6 mice stimulated for 0–72 h with TCR-CD28 and then stained with anti-p50, anti-RelA, anti-p52 and anti-RelB, followed by secondary Alexa Fluor 488–labeled (green) or Alexa Fluor 568–labeled (red) anti-mouse or anti-rabbit IgG. M, merged images. Original magnification, ×630. Results are representative of two independent experiments.

responses and related cytokine production but also to induction of autoimmune disease after transfer into *Rag2*$^{-/-}$ hosts.

## DISCUSSION

For T cells, primary immune responses generally require the classical NF-κB1 pathway[43]; whether T cell activation also requires the non-classical NF-κB2 pathway is less clear. Nevertheless, studies of NIK-deficient aly/aly mice have led to the conclusion that 'optimal' activation of mature T cells requires signaling via NIK as well as PKC-θ[13]. Because NIK controls processing of p100 to p52, it would seem to follow that T cell activation is partly dependent on nonclassical NF-κB2. However, the T cell defects in aly/aly mice also correlate with reduced spleen cell expression of p50, RelA and c-Rel[13,29], suggesting an indirect effect on the classical NF-κB1 pathway.

Here we have shown that the relative contributions of NF-κB1 and NF-κB2 to T cell activation are crucially dependent on whether the cells are immunologically naive. We have made two main points in this context. The poor immune response of total aly/aly T cells (equally true for NIK-deficient *Map3k14*$^{-/-}$ and *Relb*$^{-/-}$ cells) does not reflect a positive requirement for NF-κB2 but instead reflects the inhibitory function of a unique population of 'suppressor' cells in the total cell population. However, when depleted of those suppressor cells, the aly/aly naive T cell samples showed their cell-intrinsic 'defect' of hyper-reactivity after TCR stimulation. Thus, the aly, NIK-deficient and *Relb*$^{-/-}$ phenotype is actually a combination of a cell-extrinsic suppressor function in a subset of CD44$^{hi}$CD4+ NIK-deficient T cells and a cell-intrinsic hyperactivation response in naive CD4+ T cells that lack NIK function.

For wild-type mice, it is well established that primary responses of T cells can be suppressed by a population of CD25+Foxp3+CD4+ $T_{reg}$ cells and are enhanced when $T_{reg}$ cells are eliminated[38–40]. For aly/aly T cells, the enhancing effect of removing CD25+CD4+ $T_{reg}$ cells was much less pronounced, probably because the proportion of the NIK-deficient CD25+CD4+ $T_{reg}$ cells (specifically Foxp3+ cells) is only 20–30% of the number of such cells in wild-type mice. However, the aly/aly CD25+CD4+ $T_{reg}$ cells are suppressor cells functionally, as after enrichment they suppressed the proliferation of naive T cells nearly as well as $T_{reg}$ cells from control mice. In addition, cytokine production by $T_{reg}$ cells from aly/aly and control mice was comparable. Hence, except for an overall reduction in

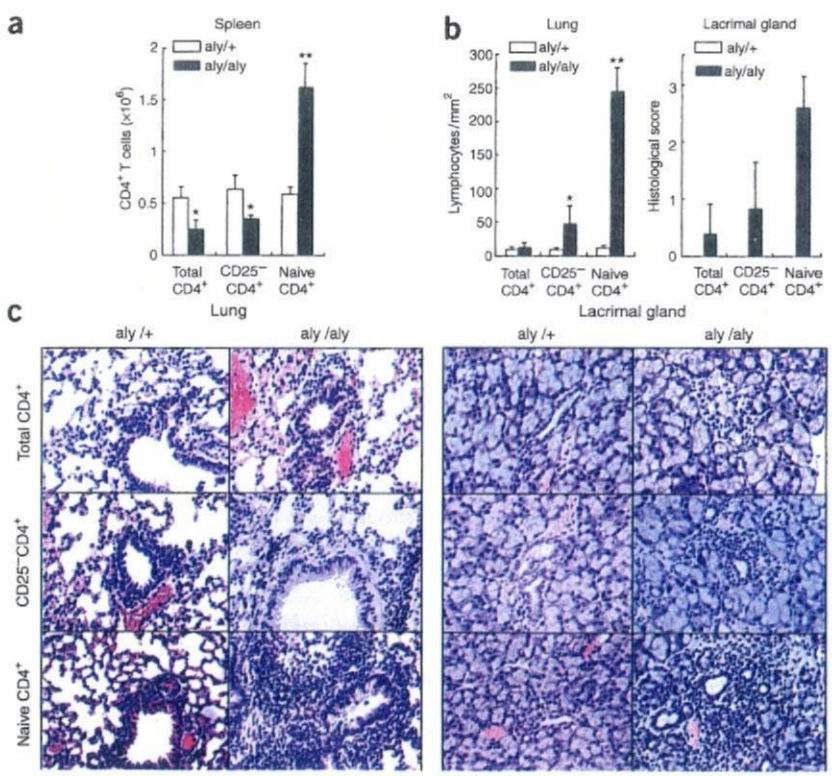


**Figure 7** Induction of autoimmune disease by subsets of aly/+ and aly/aly CD4+ cells. Enriched subsets of total CD4+, CD25−CD4+ or naive (CD25−CD44$^{lo}$) CD4+ cells from aly/+ and aly/aly mice were transferred into *Rag2*$^{-/-}$ hosts ($5 \times 10^6$ cells/mouse); mice were killed 4 weeks after transfer. (**a**) Total number of CD3+CD4+ splenocytes. Data are means ± s.d of four to five mice. *, $P < 0.05$, and **, $P < 0.005$, aly/aly versus aly/+ cells in each group. (**b**) Histopathological analysis of lung and lacrimal gland sections. Left, number of lymphocytes/mm$^2$ of lung; right, pathological score of inflammatory lesions of lacrimal glands. Data are means ± s.d. of four to five mice. (**c**) Histology of lungs and lacrimal gland sections stained with hematoxylin and eosin. Original magnification, ×100. Results are representative of four to five mice in each group.